RMetS
Royal Meteorological Society

Summer monsoon convection in the Himalayan region: Terrain and land cover effects†

Socorro Medina,[a]* Robert A. Houze, Jr.,[a] Anil Kumar[b,c] and Dev Niyogi[c]
[a]*Department of Atmospheric Sciences, University of Washington, Seattle, Washington, USA*
[b]*National Center for Atmospheric Research, Boulder, Colorado, USA*
[c]*Departments of Agronomy and Earth & Atmospheric Sciences, Purdue University, West Lafayette, Indiana, USA*
*Correspondence to: Socorro Medina, Department of Atmospheric Sciences, Box 351640, University of Washington, Seattle, WA 98195-1640, USA. E-mail: socorro@atmos.washington.edu
†This article was published online on 6 April 2010. An error was subsequently identified. This notice is included in the online and print versions to indicate that both have been corrected, 14 April 2010.

During the Asian summer monsoon, convection occurs frequently near the Himalayan foothills. However, the nature of the convective systems varies dramatically from the western to eastern foothills. The analysis of high-resolution numerical simulations and available observations from two case-studies and of the monsoon climatology indicates that this variation is a result of region-specific orographically modified flows and land surface flux feedbacks.

Convective *systems containing intense convective echo* occur in the western region as moist Arabian Sea low-level air traverses desert land, where surface flux of sensible heat enhances buoyancy. As the flow approaches the Himalayan foothills, the soil may provide an additional source of moisture if it was moistened by a previous precipitation event. Low-level and elevated layers of dry, warm, continental flow apparently cap the low-level moist flow, inhibiting the release of instability upstream of the foothills. The convection is released over the small foothills as the potentially unstable flow is orographically lifted to saturation.

Convective *systems containing broad stratiform echo* occur in the eastern Himalayas in association with Bay of Bengal depressions, as strong low-level flow transports maritime moisture into the region. As the flow progresses over the Bangladesh wetlands, additional moisture is extracted from the diurnally heated surface. Convection is triggered as conditionally unstable flow is lifted upstream of and over the foothills. The convective cells evolve into mesoscale convective systems (MCSs) with convective and stratiform areas. The MCSs are advected farther into the Himalayan eastern indentation, where orographic lifting enhances the stratiform precipitation.

Key Words: Asian monsoon; surface heat flux gradients; precipitating systems; convective systems; mesoscale simulation; orography

Received 13 November 2008; Revised 15 January 2010; Accepted 8 February 2010; Published online in Wiley InterScience 6 April 2010

Citation: Medina S, Houze RA, Kumar A, Niyogi D. 2010. Summer monsoon convection in the Himalayan region: Terrain and land cover effects. *Q. J. R. Meteorol. Soc.* **136**: 593–616. DOI:10.1002/qj.601

1. Introduction

During the South Asian monsoon (June–September), convection occurs frequently in locations where moisture flows into the subcontinent from the Arabian Sea and Bay of Bengal. Houze *et al.* (2007) (hereafter H07) and Romatschke *et al.* (2010) have shown that the location of occurrence of the most extreme convection is closely related to the unique

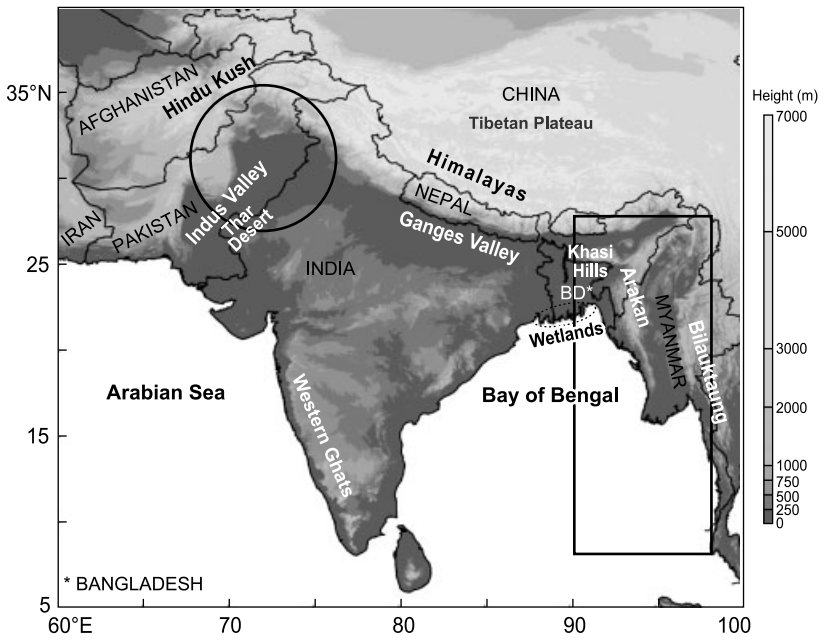

Figure 1. Orography, relevant geographical locations and regions of frequent occurrence of *systems containing intense convective echo* (circle) and convective *systems containing broad stratiform echo* (rectangle).

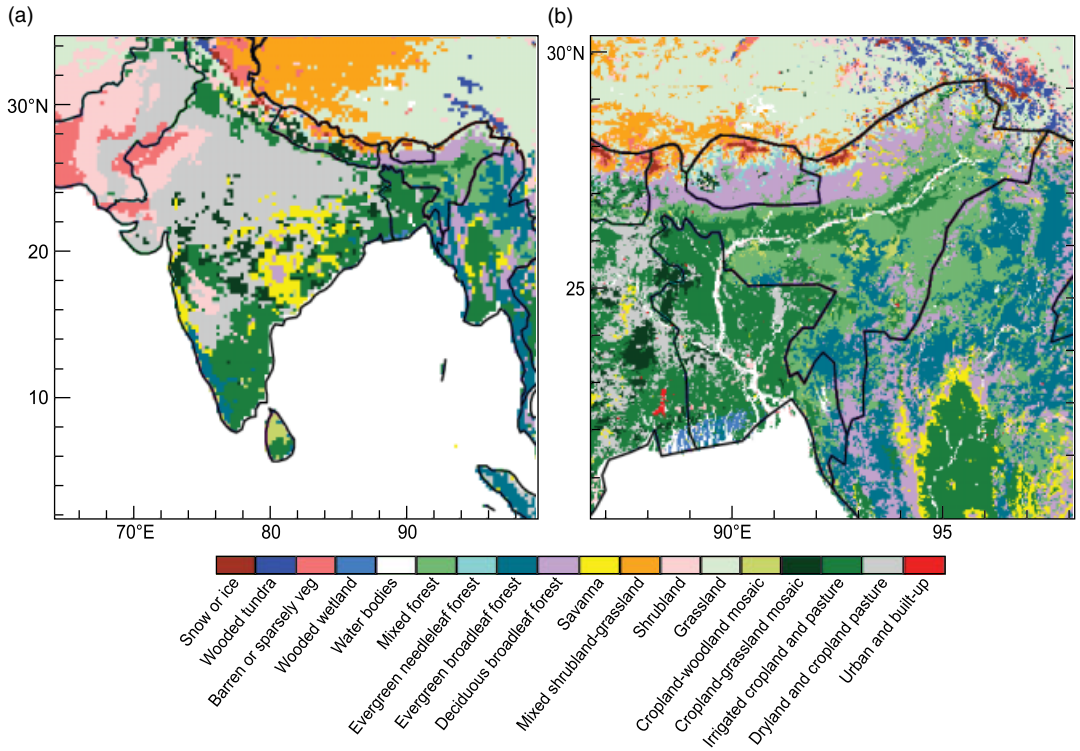

Figure 2. (a) Land cover as represented in our WRF simulations. (b) As in (a) but over the eastern Himalayas.

topography of the region. They have further suggested that the land surface conditions underlying the moist flows may affect the form taken by the convection and that the terrain plays a key role in releasing and enhancing the convection. The main geographic features of the South Asian region identified by H07 and key to this study are summarized in Figures 1 and 2, and they are:

- Sharp gradients of topography, where the Ganges and Indus Plains rise sharply to the Himalayas and other major mountain ranges.
- Relatively barren land in the northwestern portion of the subcontinent, where the Thar Desert is located.
- Moist, vegetated land surface in the eastern region, characterized by irrigated crops, pasture, and wooded wetlands at low elevations and forest over the higher terrain. Prominent in this area are the Ganges Delta and Bangladesh wetlands.

H07 and Romatschke *et al.* (2010) analysed radar echoes using Tropical Rainfall Measuring Mission (TRMM) Precipitation Radar (PR) data. They focused on two types of extreme convection: *systems containing intense convective*

echo, which are contiguous three-dimensional (3D) echo volumes that are classified as convective and have reflectivity values $\geqslant$40 dBZ, and *systems containing broad stratiform echo*, which are contiguous 3D echo volumes that are classified as stratiform and exceed 50 000 km^2 in area. They found that the form taken by extreme monsoon convective systems differs distinctly between the dry northwestern subcontinent and the moist eastern Ganges region. In the western indentation of the Himalayas (indicated by the circle in Figure 1) convective *systems containing intense convective echo* occur frequently. H07 described two categories of intense convective echo: 'deep intense echoes' (40 dBZ radar reflectivity >10 km in height[†]) and 'wide intense echoes' (40 dBZ radar reflectivity >1000 km^2 in area). Both categories have a maximum frequency of occurrence in the western indentation of the Himalayas. Meanwhile, on the eastern side (black solid rectangle in Figure 1), they found a maximum frequency of occurrence of convective *systems containing broad stratiform echo*. We refer to the northernmost part of this latter region as the eastern indentation of the Himalayas. These results led H07 to make several empirically-based hypotheses regarding how the land surface conditions modify the airflow feeding the convection and how the mountains are key in the release and enhancement of the convection.

H07 hypothesized that convective *systems containing intense convective echo* (both 'deep' and 'wide') tend to occur near the western indentation as a result of the following circumstances:

- Low-level flow that is moistened by its passage over the Arabian Sea
- The moist low-level flow is warmed by sensible heat flux as it passes over the hot and arid Thar Desert, increasing its buoyancy
- Dry flow that arrives from the Afghan or the Tibetan plateaus caps the moist low-level flow and prevents the premature release of convective instability upstream of the foothills
- Deep convection is eventually triggered when the potentially unstable low-level flow is subjected to orographic lifting over the Himalayan foothills

This set of conditions is reminiscent of those leading to severe convection over the US Great Plains, which is controlled by dry flow off the Mexican Plateau capping moist flow from the Gulf of Mexico (Carlson *et al.*, 1983).

H07 noted that the convective *systems containing broad stratiform echo* tend to be associated with Bay of Bengal depressions (e.g. Ramage, 1971; Godbole, 1977; Sikka, 1977; Houze and Churchill, 1987; Goswami, 1987) that propagate northward during active periods of the monsoon (Webster, 2006). They proposed the following hypotheses to explain the common occurrence of these precipitating systems in the region of the eastern indentation:

- The monsoonal flow is moistened by its passage over the Bay of Bengal
- As the monsoonal flow moves inland, it passes over the Bangladesh wetlands and Ganges Delta, where it further increases its moisture content
- The gentle and widespread upward motions of the synoptic system provide a moist environment favourable to the development of mesoscale convective systems (MCSs)
- As the large stratiform components of the MCSs encounter the eastern portion of the Himalayas and other mountains on the eastern side of the Bay of Bengal, the stratiform rainfall is enhanced by orographic lifting

Since the previous studies were completely empirical, based on satellite and reanalysis data, they could only hypothesize these processes. To test these hypotheses and determine physically how the topography and land surface conditions together affect the moist flow and control the formation of extreme convection in the South Asian monsoon, a high-resolution regional model is needed.

The objective of this paper is to test, quantify and refine the hypotheses proposed by H07 regarding the roles that the terrain and the land cover play in modulating the formation of monsoon convective systems in the Himalayan region. To accomplish this objective, a high-resolution regional model is needed. We draw upon the dataset of H07 to identify and select two case-studies representing typical examples of extreme convection over the western and eastern regions. These relevant case-studies are then simulated with the Weather Research and Forecasting (WRF) numerical model. The simulations are carefully evaluated using the available observational data. After determining that the model was able to produce realistic simulations, we use the model output in combination with observations to test the hypotheses outlined above. We thus use the model as a diagnostic tool to enable better physical understanding of the different forms of extreme convection that occur in the monsoon. To determine the representativeness of these results we compare the environmental conditions that existed during the simulated cases with those observed on average during the monsoon season.

2. Climatology of the monsoon

In this section, we review some of the important climatological features of the monsoon to be able to put the individual cases (sections 5 and 6) into larger context. During the monsoon, the precipitable water (i.e. vertically integrated water vapour) is maximum over the Bay of Bengal and the Arabian Sea (blue contours in Figure 3(a)). Over these bodies of water, the surface latent heat fluxes contribute to the boundary-layer moisture through evaporation (Figure 3(c)). The prevailing low-level southwesterly winds extract moisture from the ocean and transport it towards the Indian subcontinent (Figure 3(a)). As has been shown by Hirose and Nakamura (2002), Xie *et al.* (2006) and others, as the moist flow approaches the land, maxima of precipitation occur upstream and over the lower windward slopes of the west- and south-facing mountain barriers (i.e. Western Ghats, Arakan, Bilauktaung and Himalayan Mountains, Figure 1) (Figure 3(b)).

Upon landfall, the flows advancing from the Arabian Sea and the Bay of Bengal encounter dramatically different land surfaces and hence the surface heat fluxes are very different between these two regions (Niyogi *et al.*, 2002; Douglas *et al.*, 2006). The surface latent heat flux, which results from evapotranspiration, has a local maximum south of

[†]Unless otherwise stated, all heights are above mean sea level (MSL).

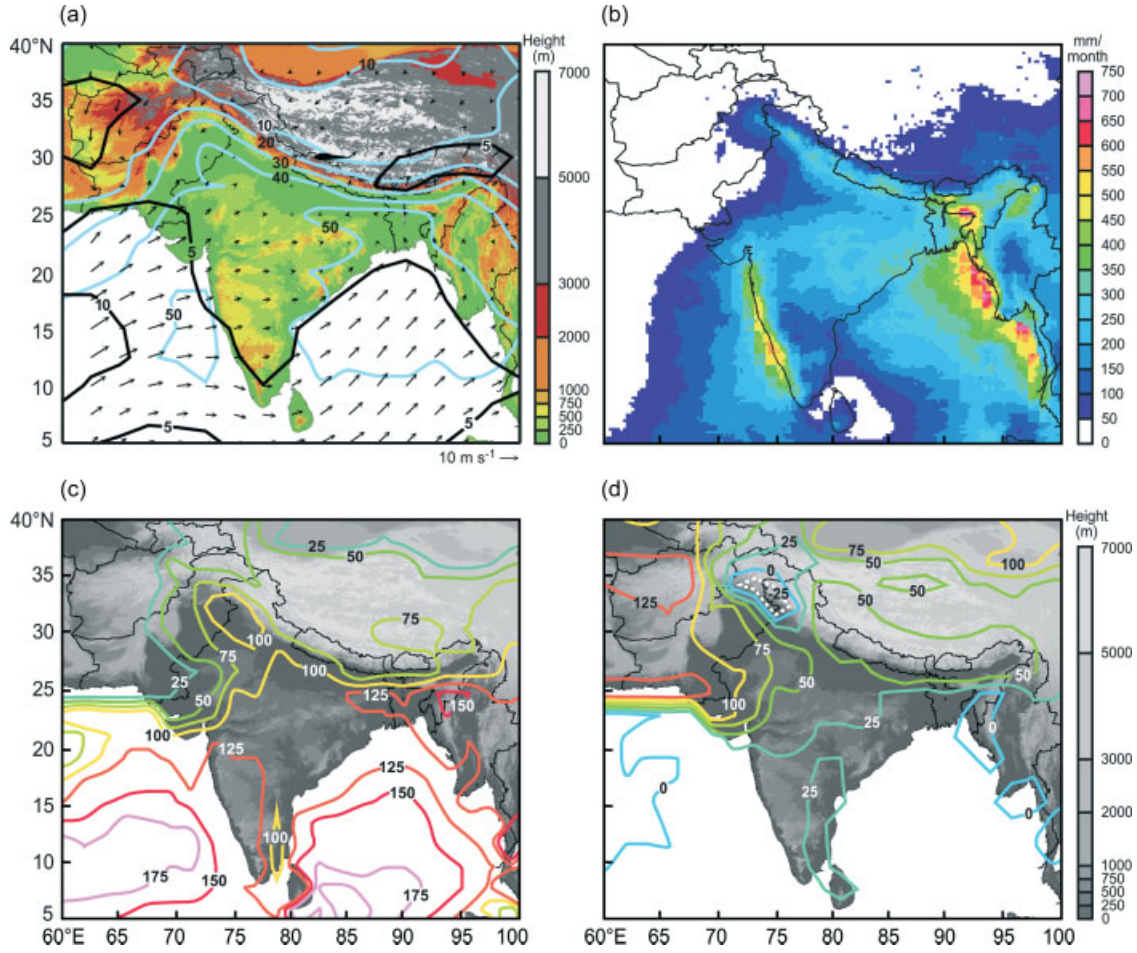

Figure 3. June to September climatological fields. Except for panel (b), the data are from NCEP reanalysis. (a) Surface wind vectors, precipitable water (mm, blue contours), and surface wind speed (m s^{-1}, black contours). (b) Precipitation climatology (from 1998–2007 TRMM 3B43 product). Surface fluxes of (c) latent heat and (d) sensible heat (W m^{-2}). Negative contours are dashed. The orography is shown by colour shading in (a) and by grey shading in (c) and (d).

the eastern Himalayas (Figure 3(c)), where the land surface is characterized by irrigated cropland, wetlands, and forests (Figure 2). In contrast, a local minimum in surface latent heat flux is seen near the Thar Desert, where the surface sensible heat flux dominates (Figure 3(d)). The minimum in surface latent heat flux seen over the Thar Desert (Figure 3(c)) does not extend farther downstream (i.e. to the northeast), as the region downstream is characterized by frequent convection (circle in Figure 1). This region is also characterized by negative surface sensible heat flux (Figure 3(d)) as the extremely hot low-level air that previously resided over the Thar Desert moves over the relatively cooler surface of the western indentation, which is on average characterized by moister soil.

The low moisture content observed in Afghanistan and western Pakistan (Figure 3(a)) is part of a large-scale feature that extends throughout North Africa and the Middle East (e.g. Fig. 5b of Annamalai *et al.* (1999)). As a result, there are strong moisture gradients near the India–Pakistan border that separate moist monsoonal air over the Indian Peninsula from the dry air that pervades North Africa and the Middle East. These gradients are observed at all levels of the atmosphere, up to 400 mb (not shown).

3. Observational datasets

This study uses the following observational datasets:

- Synoptic maps based on reanalyses of the Indian National Centre for Medium Range Weather Forecasting (NCMRWF) global T80 model (Rajagopal *et al.*, 2001; Goswami and Rajagopal, 2003)
- Sounding data obtained through the University of Wyoming (http://weather.uwyo.edu/upperair/)
- Infrared satellite imagery from Meteosat 5 obtained from the European Organization for the Exploitation of Meteorological Satellites (EUMETSAT, http://www.eumetsat.int/)
- Radar data from the Tropical Rainfall Measuring Mission Precipitation Radar (TRMM PR). The gridded, attenuation-corrected three-dimensional reflectivity fields (Version 6 of product 2A25: Iguchi *et al.*, 2000a, 2000b) were remapped as described by H07
- TRMM monthly precipitation estimates (product 3B43: Adler *et al.*, 2000; Huffman *et al.*, 2007) from 1998 to 2007 were used to calculate the monsoon precipitation climatology
- National Oceanic and Atmospheric Administration (NOAA) Air Resources Laboratory (ARL) Hybrid single-particle Lagrangian integrated trajectory (HYSPLIT) model output (http://www.arl.noaa.gov/ready/hysplit4.html) computed using model vertical velocity and based on National Centers for Environmental Prediction Global Final Analysis (NCEP FNL) data

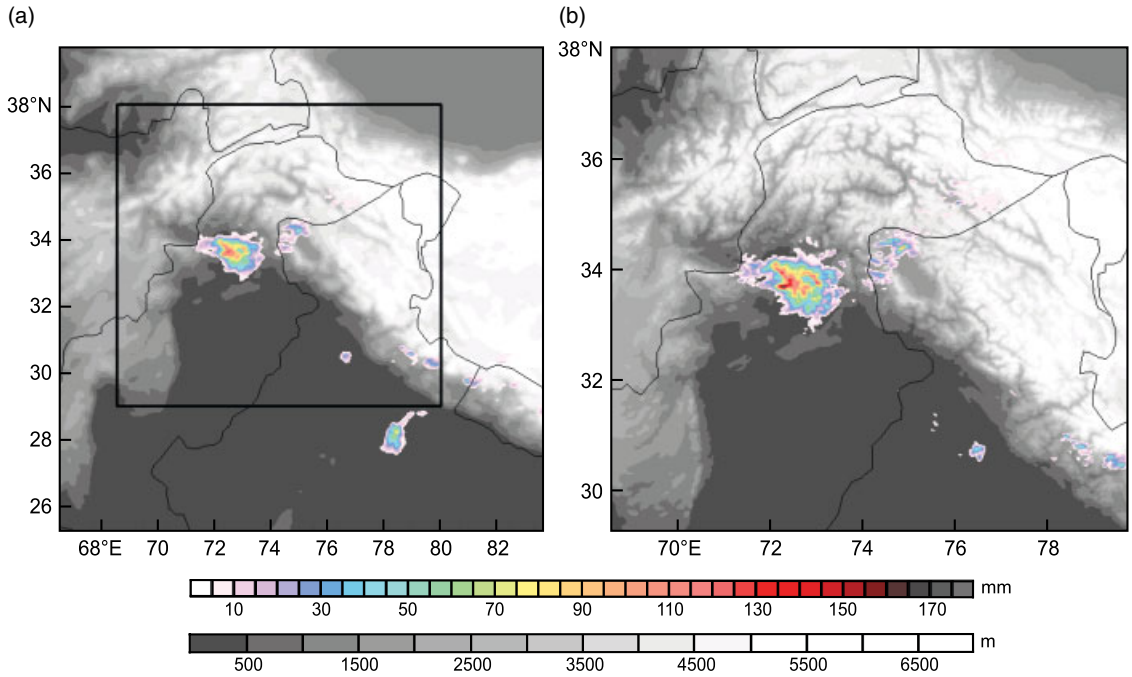

Figure 4. Domains used to simulate a *system containing intense convective echo*. The terrain (grey shading) and accumulated precipitation (colour shading) throughout the simulation (1800–2300 UTC 3 September 2003 (2300 LST 3 September–0400 LST 4 September 2003)) are shown for (a) Domain 1 (horizontal resolution = 9 km) and (b) Domain 2 (horizontal resolution = 3 km).

- NCEP reanalysis (Kalnay *et al.*, 1996). From the NCEP reanalysis, we will use meteorological and surface heat fluxes[‡]

4. General model description

The simulations in this paper were carried out with the Advanced Research Weather Research and Forecasting (WRF) model version V2.1.1 (Skamarock *et al.*, 2005; http://www.mmm.ucar.edu/wrf/users/). The initial and boundary conditions for the large-scale atmospheric fields, sea-surface temperature (SST), as well as soil parameters (moisture and temperature) are given by the 1×1 degree 6-hourly NCEP FNL data available from http://dss.ucar.edu/datasets/ds083.2/. These data were interpolated to the respective WRF grid using Standard Initialization (WRFSI, http://wrfsi.noaa.gov/gui).

Kumar *et al.* (2008) and Chang *et al.* (2009) tested a number of WRF model configurations for improved simulation of convection and rainfall over the Indian monsoon region. The simulations presented here are based on their results and use the physical parametrizations that give the most realistic results. Our simulations were conducted using the WRF single-moment (WSM) 6-class bulk microphysical parametrization (BMP) scheme (WSM-6: Hong *et al.*, 2004; Hong and Lim, 2006). The WSM-6 scheme consists of mixing ratio tendency equations for vapour, cloud water, cloud ice, rain, graupel and snow. The Betts–Miller–Janjić (BMJ) cumulus parametrization scheme, based on the Betts–Miller convective adjustment scheme (Betts, 1986; Betts and Miller, 1986), was also used.[§] A 5-layer thermal diffusion land-surface scheme was used in order to account for the surface feedback based on soil temperature. This scheme is based on the fifth-generation Pennsylvania State University-National Center for Atmospheric Research Mesoscale Model (MM5) 5-layer soil temperature model (Dudhia, 1996). The five layers are 1, 2, 4, 8 and 16 cm thick, and below these layers the temperature is constant. The scheme allows for a snow-cover flag and its energy budget includes sensible and latent heat fluxes as well as radiation. The Yonsei University scheme of Hong and Pan (1996) was used to represent the Planetary Boundary layer (PBL). For long-wave radiation calculations, the Rapid Radiative Transfer Model (RRTM: Mlawer *et al.*, 1997) was used. The short-wave radiation calculation is based on Dudhia (1989).

The simulations were conducted using one- and two-way WRF nesting methods (provided in detail at http://www.wrf-model.org) and are described in sections 5 and 6. The vertical structure was represented by 31 layers and a terrain-following hydrostatic-pressure vertical coordinate, which varied from a value of 1 at the surface to 0 at the upper boundary of the model domain (Skamarock *et al.*, 2005).

[‡]While the uncertainties in the NCEP reanalysis meteorological fields are relatively well known (e.g. Goswami and Sengupta, 2003), the uncertainties of the NCEP surface heat fluxes are not as well documented, especially over southern Asia, which is characterized by sparse data availability. However, recent studies using data from individual buoys have found that over the southeastern Arabian Sea, the discrepancy between *in situ* observed and NCEP surface latent and sensible heat fluxes is ~50 W m^{-2} and ~12 W m^{-2}, respectively (Swain *et al.*, 2009), while over the southern Indian Ocean they are ~20 W m^{-2} and ~2 W m^{-2}, respectively (McPhaden *et al.*, 2009, their Fig. 11).

[§]In our simulations, a very small fraction of the total precipitation was produced by the cumulus parametrization scheme.

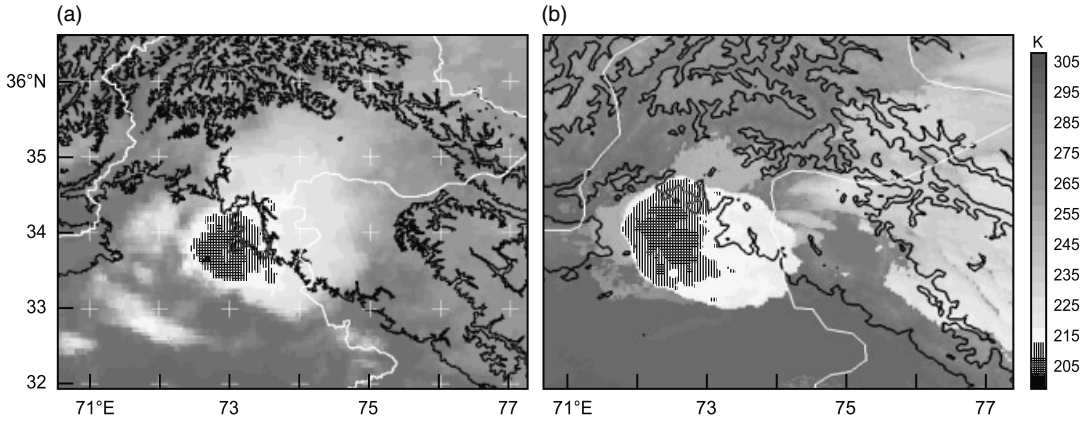

Figure 5. (a) Observed infrared satellite temperature, and (b) simulated (from Domain 2) cloud-top temperature for a *system containing intense convective echo* (2130 UTC 3 September 2003). The 1 and 4 km terrain contours are shown in black.

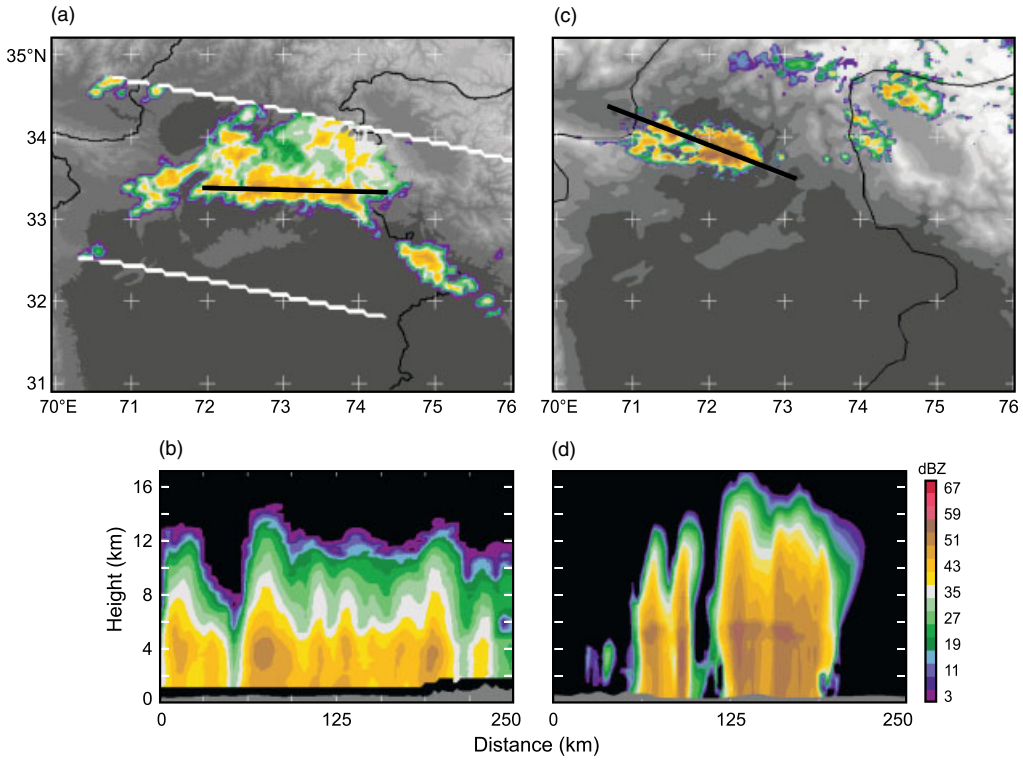

Figure 6. Reflectivity for a *system containing intense convective echo* as (a)–(b) observed by TRMM at 2200 UTC 3 September 2003 and (c)–(d) simulated (Domain 2) at 2000 UTC 3 September 2003. Panels (a) and (c) show horizontal cross-sections at 4 km. Panels (b) and (d) show vertical cross-sections taken along the black lines in panels (a) and (c), respectively. Observed panels adapted from H07.

5. A typical example of a *system containing intense convective echo* in the northwestern subcontinent

5.1. Simulation details

In order to understand the frequent occurrence of *systems containing intense convective echo* in the western Himalayan indentation (circle in Figure 1), we simulated a typical event observed in this region. We have chosen a typical convective system containing a 'wide convective echo' (defined by H07 as having a 40 dBZ echo exceeding 1000 km^2 in area). This case was observed by TRMM around 2200 UTC 3 September 2003. Two nested domains, centred near the location of the TRMM radar echo, were used to simulate this case (Figure 4). The model orography and accumulated precipitation throughout the simulation are shown in Figure 4. Domain 1 has a horizontal resolution of 9 km and the resolution for Domain 2 is 3 km. Two-way nesting was employed. Domain 2 obtains its initial and boundary conditions from Domain 1. The simulation, initialized at 1800 UTC 3 September 2003 and run for 5 h (from 2300 Local Standard Time (LST)** 3 September to 0400 LST 4 September 2003), depicted a night-time event.

5.2. Simulation evaluation

The timing and location of the system were captured by the simulation, with the simulated cold cloud shield slightly larger than the observed one (Figure 5). Figure 6 compares

**The LST in Pakistan, where this case was observed, is UTC + 0500.

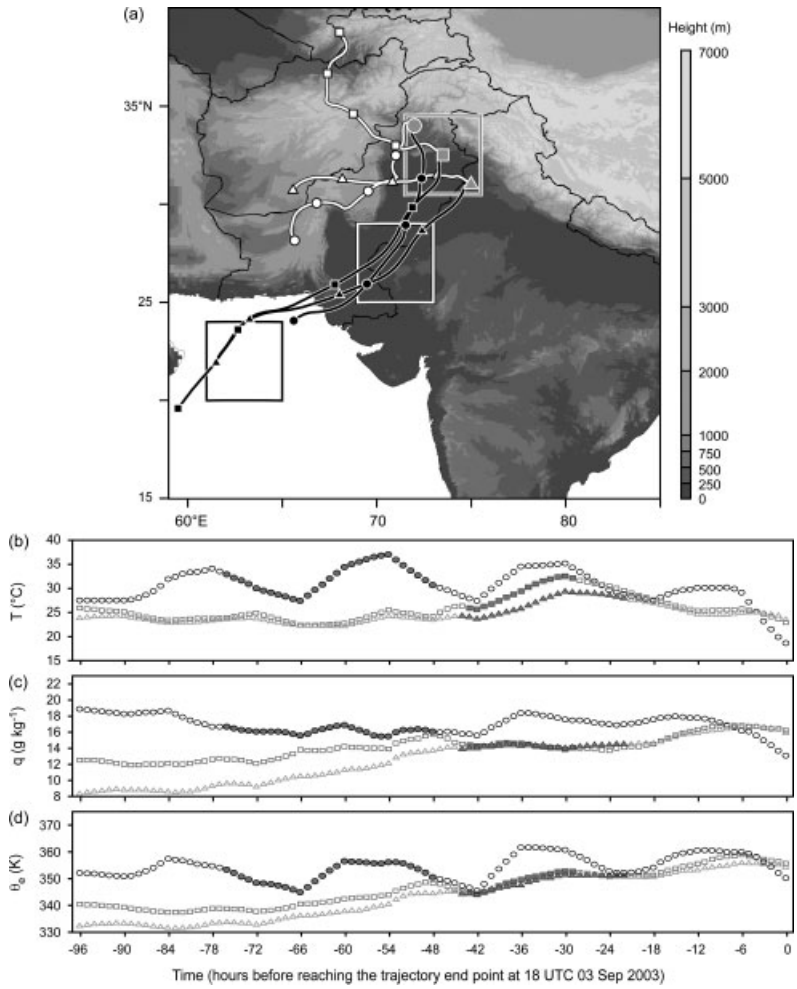

Figure 7. FNL backward trajectories coinciding with the occurrence of a *system containing intense convective echoes.* (a) Trajectories for parcels reaching the locations indicated by the grey symbols at 1800 UTC 3 September 2003 at 3.0 km AGL (white trajectories) and 1.0 km AGL (black trajectories). The circle, square and triangle markers are used to identify each trajectory. The time elapsed between markers is 24 h. The large squares identify the regions of the Arabian Sea, the Thar Desert, and the western terrain indentation used in Figure 10. (b)–(d) Time series of temperature, water vapour mixing ratio, and equivalent potential temperature, respectively, for the low-level trajectories shown in (a). The solid symbols identify the period when the low-level trajectories were over the Thar Desert.

the only available snapshot of TRMM PR reflectivity data obtained in this case with the simulated radar reflectivity[††] at a time when the observed and simulated systems are apparently in a similar stage of development. The simulated precipitation does not extend as far east as the observed system, but its intensity, location and shape compare relatively well with the observations (Figure 6(c) and (a)). Vertical cross-sections along the system show that in both observations and simulation the precipitation is characterized by vertically upright convective echoes (Figure 6(b) and (d)), structures typical of this region (H07). The convective echoes are deeper in the simulation, probably partly the result of the TRMM PR 17 dBZ sensitivity[‡‡], and partly model overestimation of the depth of the echoes. However, the simulation is considered realistic enough given: (1) all the assumptions involved in deriving reflectivity and (2) that the simulated system eventually developed an area of stratiform precipitation, which was also seen in the northeastern edge of the observed system (Figure 6(a)).

Since the overall structure of the system was captured by the simulation, the model output, along with NCEP data, will be used to test the individual hypotheses put forward by H07. The source of the information used, whether observed data or simulated output, is clearly indicated in all the figure captions.

5.3. *Moist low-level flow from the Arabian Sea is capped by dry and warm flow*

H07 hypothesized that in *systems containing intense convective echoes*, like the one observed on 3 September 2003, low-level moist southerly flow moved from the Arabian Sea towards the land, where it was capped by dry air flowing off the Afghan or Tibetan plateaus. They suggested that the cap prevented the release of convective instability upstream of the foothills. These hypotheses will be tested in this subsection.

[††]The simulated reflectivity calculations were conducted using the Read Interpolate Plot (RIP) software, version 4.3. These calculations were conducted consistently with the WSM-6 BMP scheme, using constant intercept parameters for rain and graupel and a temperature-dependent intercept parameter for snow (Hong *et al.*, 2004; Hong and Lim, 2006). To simulate the radar bright band (Houze, 1997), frozen particles at temperatures above freezing are assumed to scatter as liquid particles (Stoelinga, 2007, personal communication).

[‡‡]The observed values less than 17 dBZ arise as a result of the Cartesian interpolation (H07).

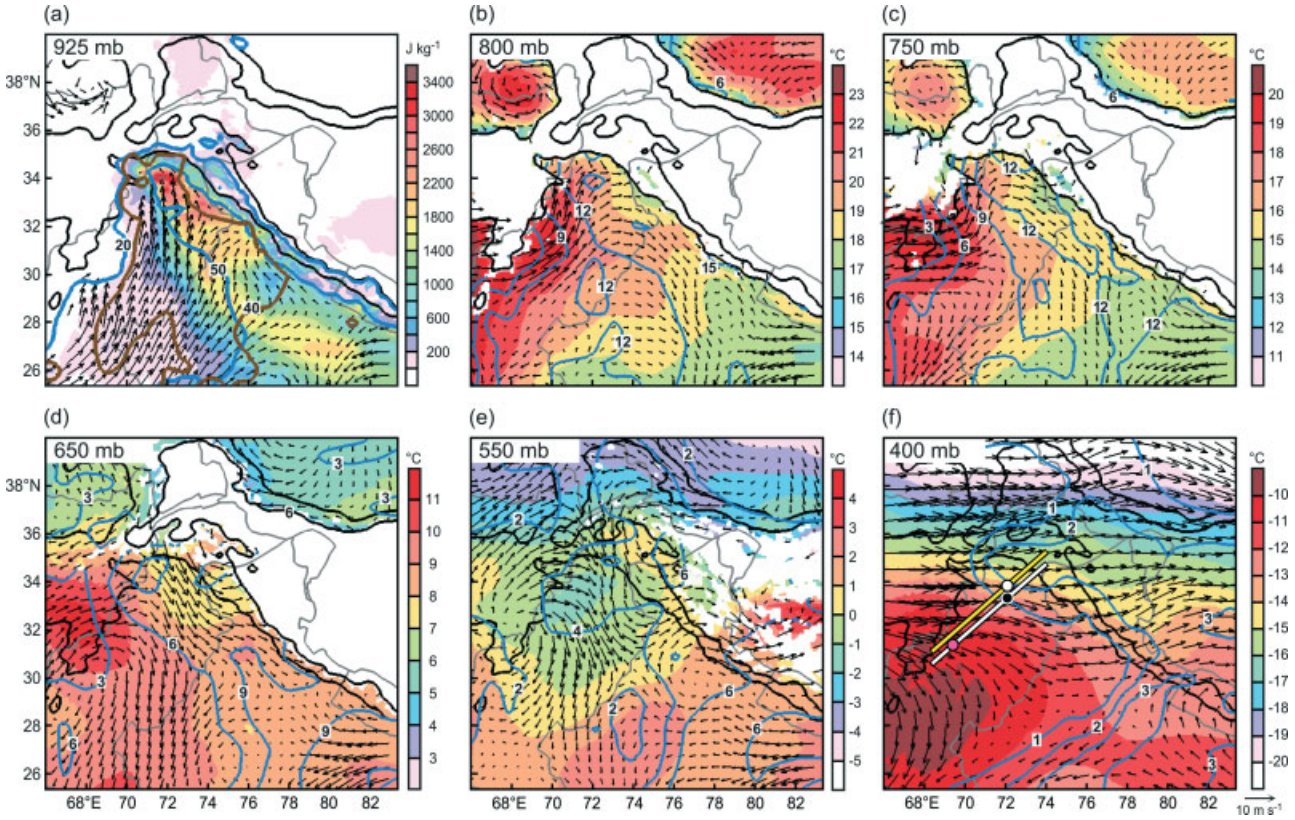

Figure 8. Simulated variables during a *system containing intense convective echoes* (1800 UTC 3 September 2003). (a) Precipitable water (mm, blue contours), CIN (brown contour), CAPE (colour shading), and 925 mb wind vectors. (b)–(f) Temperature (colour shading), water vapour mixing ratio (g kg^{-1}, blue contours) and wind vectors at pressure levels of 800, 750, 650, 550 and 400 mb, respectively. The black contours show the 2 and 4 km (slightly smoothed) terrain isolines. Panel (f) indicates the location of cross-sections and soundings discussed in the text. The white circle marks the location where convection eventually initiated. All fields are from Domain 1.

First, we analyse the origin of the parcels in the air column that reached the western terrain indentation immediately before convective initiation. Since the convection develops very quickly (∼1 h) after model initiation (section 5.5), it is not possible to obtain a mesoscale WRF simulation that extends far enough back in time to trace the regions of origin of the parcels. Instead, NOAA ARL HYSPLIT model backward trajectories were constructed using NCEP FNL data. Backward trajectories were conducted from three end points located near the terrain indentation (grey solid symbols in Figure 7(a)). The circle, square, and triangle symbols are used throughout Figure 7 to identify each trajectory. The end time of the backward trajectories is 1800 UTC 3 September 2003, i.e. ∼1 h before convection initiation (section 5.5). The parcels that ended at 3.0 km above ground level (AGL) resided over the Hindu Kush mountains of Afghanistan two to four days before reaching the end points (white lines in Figure 7(a)). In contrast, three to four days before reaching the end points, the low-level (1.0 km AGL) parcels resided over the moist Arabian Sea (black lines in Figure 7(a)), before moving over the dry and hot Thar Desert (indicated by the white square in Figure 7(a)) and proceeding towards the Himalayan foothills.

These trajectories, with flow off the Afghan mountains above and low-level flow from the Arabian Sea, are consistent with the analyses of Sawyer (1947) and H07 of monsoon convection in this region. However the trajectories clearly indicate that the origin of the dry flow aloft is the Afghan Hindu Kush mountains, not the Tibetan Plateau. The high-resolution WRF simulation reveals the complex nature of the flow and moisture distribution. The following discussion, based on Figure 8, shows the model's representation of the atmosphere 1 h before convective initiation. The 2 and 4 km terrain contours (black lines) delimit a large flat area on the south side of the domain enclosed to the northwest and northeast by the Hindu Kush and Himalayan mountains, respectively. Panel (a) shows the precipitable water (blue contours) and the winds at 925 mb, among other fields discussed later. The remaining panels show the winds, temperature (colour shading) and water vapour mixing ratio (blue lines) at higher levels. Very low precipitable water air resided on the west side of the plains, while on the east side the air had values >50 mm (Figure 8(a)), which is apparently higher than the monsoon climatological mean (Figure 3(a)). The flow at 925 mb tended to have a strong southerly component (Figure 8(a)). Immediately above, there was dry and warm air on the west side of the plains that was flowing off and then parallel to the Hindu Kush mountains (Figure 8(b)–(c)). As this flow reached the northernmost indentation of the terrain, it was deflected and flowed parallel to the Himalayas as northwesterly flow (Figure 8(b)–(c)). At mid-levels (∼650–550 mb), the stronger winds were found near the northernmost terrain indentation, where the temperature was lower and the water vapour mixing ratio was higher than in the immediate surroundings (Figure 8(d)–(e)). At higher levels (⩽400 mb), there were strong westerlies/northwesterlies that advected dry air into the region (Figure 8(f)).

Figure 8 indicates that the air was in general drier on the west side at all levels. To study the vertical structure with more detail, we present a vertical cross-section extending from the region of dry and warm air toward the northeast

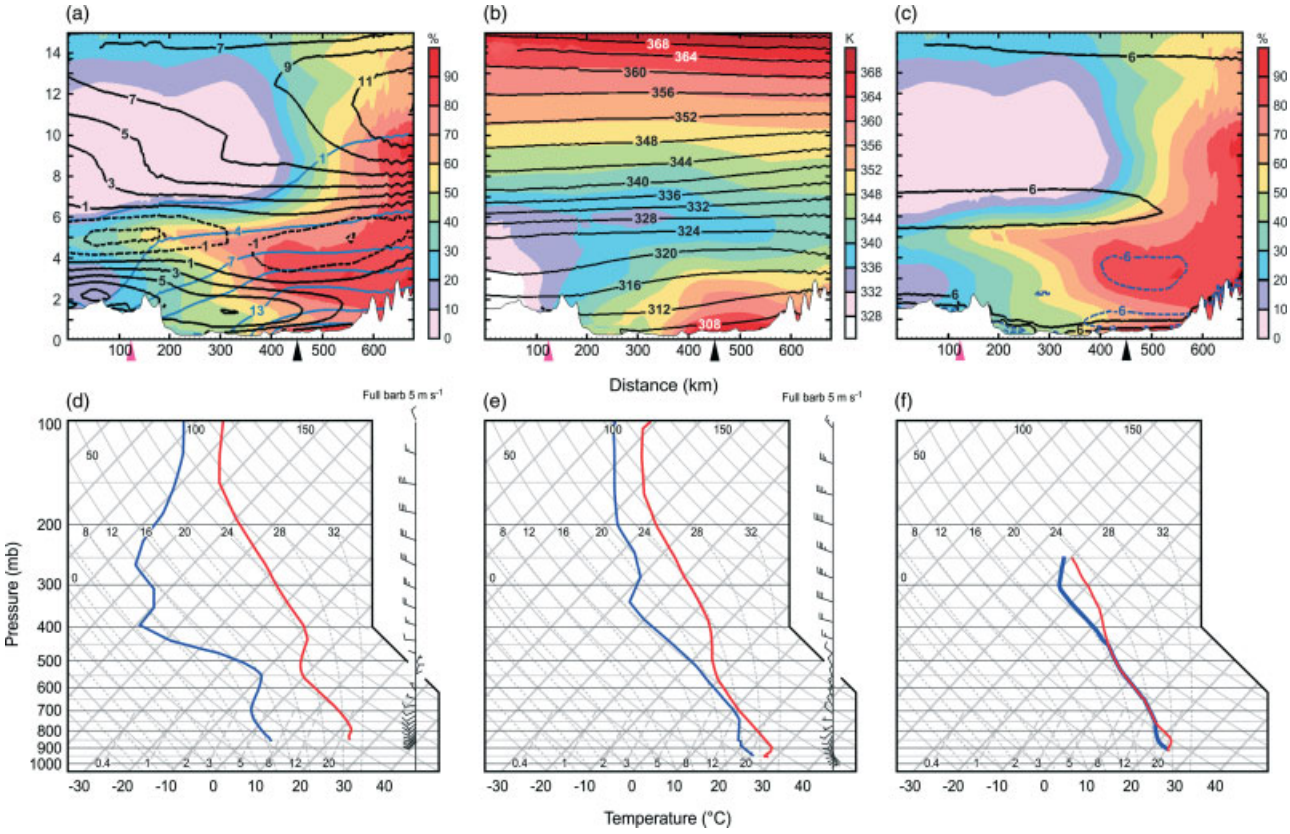

Figure 9. Simulated variables during a *system containing intense convective echoes* at (a)–(c) 1800 UTC and (d)–(f) 1825 UTC 3 September 2003. (a) Vertical cross-section along the white line in Figure 8(f) of relative humidity (colour shading), water vapour mixing ratio (g kg^{-1}, blue contours), and horizontal wind component parallel to the cross-section (m s^{-1}, black contours where solid lines indicate flow from left to right). (b) Same as (a) but showing θ_e (colour shading) and θ (black contours). (c) Same as (a) but showing dθ/dz (black contour, 6 K km^{-1} isoline) and dθ_e/dz (blue contour, -6 K km^{-1} isoline). Soundings taken at (d) the dry and warm side (at the location indicated by the magenta triangle in (a)–(c) and the magenta circle in Figure 8(f)) and (e) the moist and cold side (at the location indicated by the black triangle in panels (a)–(c) and the black circle in Figure 8(f)). (f) Stratification resulting from lifting the sounding in (e) by 50 mb. Panels (a)–(c) show the underlying terrain in white fill. All the fields are from Domain 2.

(white line in Figure 8(f)). Figure 9(a) shows that at low levels there is a tongue of low relative humidity (colour shading) air with a westerly component (black solid lines), apparently flowing downslope from the Hindu Kush mountains toward the plains in the northeast. At a distance of ∼500 km, the dry, warm downslope air protrudes between two layers of higher relative humidity: a shallow near-surface layer and a thicker layer at ∼2–5 km. The origin of this mid-level moist layer will be discussed in section 5.6. Above 6 km there are strong winds with a westerly component and relative humidity ∼10% on the western edge of the domain. The upper-level dry flow is part of a large-scale pattern, persistent throughout the monsoon season, which brings dry, continental air from the Arabian Peninsula and Iran towards the region of study (section 2). Thus, during the monsoon, the area between Pakistan and India is on average characterized by large relative humidity gradients (Annamalai *et al.*, 1999) as the extremely dry continental westerly flow reaches the longitudes where moisture is constantly transported to upper levels by monsoon convection. This gradient is manifested at heights >6 km and at a distance ∼500 km in Figure 9(a).

The distinct nature of the layers identified above is reflected in the thermodynamic and wind structure of soundings extracted on the warm/dry and cold/moist sides (at the locations indicated by the magenta and black circles in Figure 8(f), respectively). On the dry side, we see between 800–600 mb near-dry-adiabatic, dry, west-southwesterly flow (Figure 9(d)). Then there is a thin layer of relatively moister air at ∼550 mb that is separated by a stable layer at ∼475 mb from dry west-northwesterly winds aloft (Figure 9(d)). On the moist side, the sounding shows shallow and moist near-surface south-southeasterly flow, relatively drier south-southwesterly air at ∼900 mb, moist north-northwesterly flow at ∼650 mb and drier west-northwesterly flow above ∼400 mb (Figure 9(e)). The stability characteristics of these layers will be analysed in section 5.5.

This analysis suggests that are two sources of dry air near the western indentation of the Himalayas: the Hindu Kush mountains (at levels below ∼4 km) and what Sivall (1977) called a planetary-scale westerly flow (at ∼6–14 km). Between these flows there is mid-level moist monsoonal air (discussed in section 5.6). This interpretation is consistent with the conceptual model presented by Sivall (1977, his Fig. 19).

5.4. *Build-up of buoyancy via heat fluxes*

The backward trajectories indicated that the low-level parcels that ended in the western terrain indentation had resided previously over the Arabian Sea and the Thar Desert (black lines in Figure 7(a)). In this section, we explore the build-up of buoyancy via heat fluxes for these trajectories.

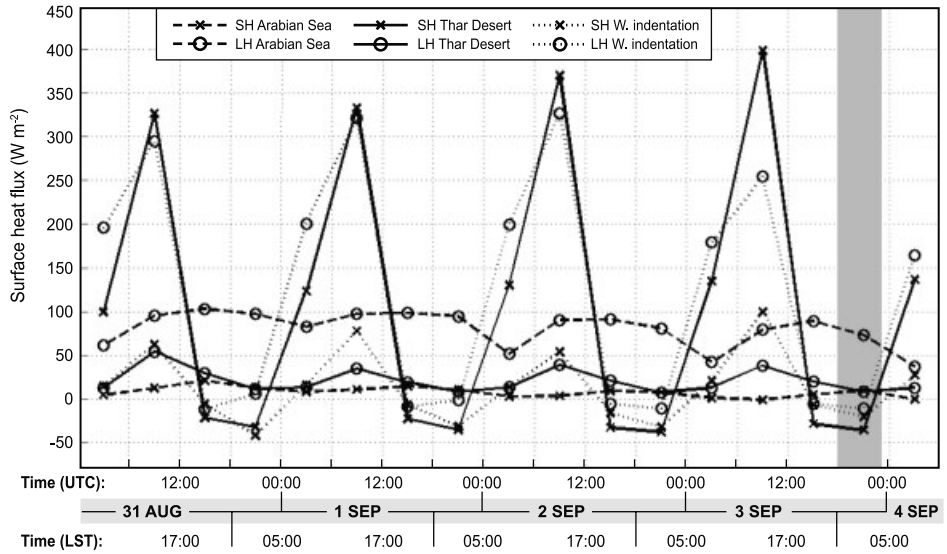

Figure 10. NCEP reanalysis time series of surface heat fluxes in the days leading up to a *system containing intense convective echoes*. The fluxes were averaged over the Arabian Sea (dashed lines), over the Thar Desert (solid lines), and near the western terrain indentation (dotted lines). The location of these regions is indicated by the large squares in Figure 7(a). The time series of surface flux of sensible (latent) heat are identified with crosses (circles). The grey bar indicates the time period of the WRF simulation.

The bottom three panels in Figure 7 show the time series of meteorological variables for the low-level trajectories in panel (a)[‡‡]. The solid symbols in panels (b)–(d) indicate the times when the trajectories were directly over the Thar Desert (white square in Figure 7(a)). Throughout its duration, the trajectory identified by the circles was located closer to the ground than the other two trajectories (except for the last 3 h) and therefore it had a stronger degree of diurnal variability, as can be seen by the larger variations in its temperature (Figure 7(b)). All the trajectories show a temperature increase as they move over the Thar Desert (Figure 7(b)). The exact timing of the temperature increase is controlled by the phase of the diurnal cycle; however, given that these parcels spent on average 21 h over the Thar Desert, i.e. nearly a full diurnal cycle, the exact timing is not relevant. The trajectories identified by the squares and triangles have a steady increase in water vapour mixing ratio as they move over the Arabian Sea (Figure 7(c)). All trajectories retain relatively constant water vapour mixing ratio values while they move over the Thar Desert. Around 7–14 h after leaving the Thar Desert, the mixing ratio tends to increase. As a result of these temperature and mixing ratio changes, the equivalent potential temperature (θ_e) in general increases as the parcels approach the Himalayan foothills (Figure 7(d)). The diurnal cycle produces fluctuations, which are more obvious for the trajectory closer to the surface (denoted by circles); however, the general trend is for θ_e to increase as these parcels approach the foothills.

To assess the magnitude of the associated surface heat fluxes, we look at the NCEP reanalysis over relevant subregions in the days leading up to the event. The fluxes were spatially averaged over the Arabian Sea (20–24°N, 61–65°E), the Thar Desert (25–29°N, 69–73°E), and the western terrain indentation (30.5–34.5°N, 71.5–75.5°E), regions indicated by the large squares in Figure 7(a). The following discussion is based on Figure 10. The grey bar indicates the time span of the WRF simulation (1800–2300 UTC 3 September). Over the Arabian Sea, the surface flux of latent heat had a relatively weak diurnal cycle and a mean value of ∼80 W m^{-2}, while the sensible heat flux was very small (dashed lines with circles and crosses, respectively). Over the Thar Desert, in contrast, the heat fluxes had a large diurnal cycle, which is characteristic of this region (Chiao and Barros, 2007). During each of the days previous to the event, the sensible heat fluxes were very large (>150 W m^{-2}) between 0600 and 1200 UTC (1100–1700 LST), dominating over the latent heat flux (solid lines with crosses and circles, respectively).

To explore the origin of the water vapour mixing ratio increase farther downstream from the Thar Desert (Figure 7(c)), we look at the heat fluxes over the western indentation. The maximum sensible heat flux attained during the daytime decreased significantly, while the latent heat flux increased considerably (dotted lines with crosses and circles, respectively) compared to the values observed over the Thar Desert. The large surface flux of latent heat over the western indentation suggests that the land in this region provides a local source of surface moisture, presumably provided by previous precipitating systems, which occur frequently in this region (H07; Romatschke *et al.*, 2010).

The analysis in this subsection suggests that the large flux of sensible heat from the Thar Desert to the atmosphere during the daytime in successive days, led to the increase of the low-level air temperature seen in Figure 7(b) over the desert. The large moisture flux from the western indentation apparently led to the increase in low-level moisture seen downstream of the Thar Desert (Figure 7(c)). These sensible and latent fluxes contributed to the θ_e increase (and implied instability build-up) seen as the flow proceeded from the Arabian Sea to the foothills (Figure 7(d)), as hypothesized by H07.

[‡‡]The variation of the height of the low-level trajectories (both above MSL and AGL) is very small for most of the time period shown in Figure 7, except for the last 18 h.

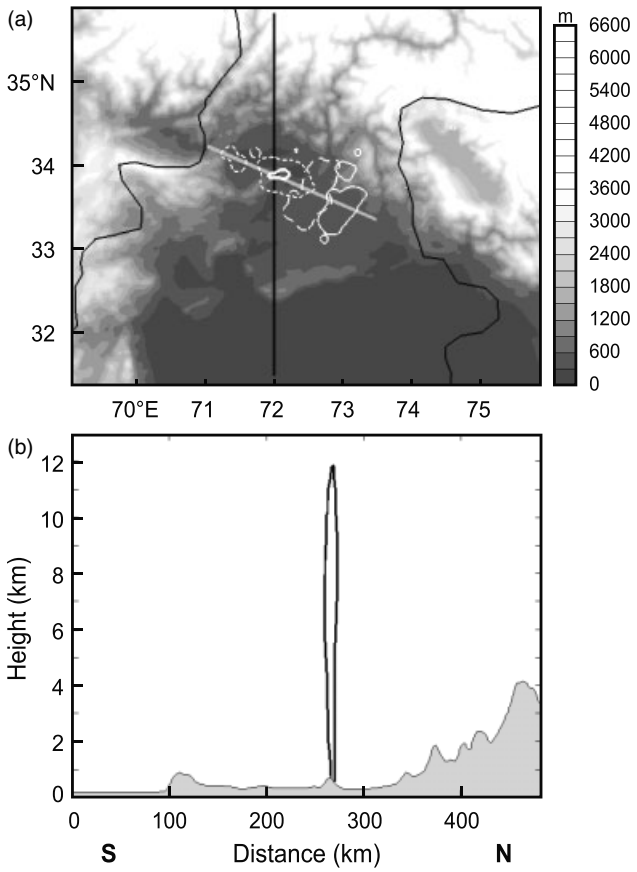

Figure 11. Simulated variables during a *system containing intense convective echoes*. (a) Terrain (grey shading) and vertically integrated mixing ratio of precipitating hydrometeors 10 mm isochrones at 1900 UTC (thick white solid contour), 2000 UTC (short dashed contour), 2200 UTC (long dashed contour), and 2300 UTC 3 September 2003 (thin solid contour). (b) Vertical cross-section of mixing ratio of precipitating hydrometeors (black contour, 1 g kg^{-1} isoline) along the south–north-oriented line in (a) at the time convection was initialized (1900 UTC 3 September 2003). The underlying terrain is shown by the grey shading. All fields are from Domain 2.

5.5. *Triggering of convection as potentially unstable air is subjected to orographic lifting*

Sawyer (1947) and H07 suggested that capping by a dry and warm layer prevents convection from easily breaking out. They further hypothesized that convection does not erupt until the low-level potentially unstable moist flow reaches the Himalayan foothills, where convection is released as a result of orographic lifting. This hypothesis is tested in this section.

We will show later that the convection initiated in the simulation at 1900 UTC 3 September 2003 at 33.89°N, 72.15°E (indicated by the white circle in Figure 8(f)). First, we assess the stability before the initiation of convection by analysing the vertical gradients of potential temperature (θ) and equivalent potential temperature (θ_e) (Figure 9(b)). Except for the southwest edge of the cross-section, θ_e decreases with height up to ∼6 km, indicating that this layer is potentially unstable and that convection would develop if the layer were subjected to enough lifting. In contrast, θ increases with height everywhere. Figure 9(c) shows the heights where the vertical gradients of θ are maxima (black contours) and those of θ_e are minima (blue dashed contours). The atmosphere consists of two strongly stable layers: a thin one near the surface and a thicker one at ∼6 km. There is a deep potentially unstable layer below 6 km. Hence convection must overcome two lids before it can develop. This is different from the situation in the US Great Plains, where only one lid exists.

The sounding in Figure 9(e) was extracted slightly to the south of the location where convection started (black circle in Figure 8(f)) 45 min before initiation. This sounding is characterized by high convective available potential energy (CAPE) (∼1775 J kg^{-1}) and some convective inhibition (CIN) (∼174 J kg^{-1}). The CAPE was very large on the eastern side of the plains (colour shading in Figure 8(a)). There was also some CIN over the plains (brown contour in Figure 8(a)), which tended to be larger on the western side. The CIN is associated with the dry and warm downslope flow from the Hindu Kush mountains, which is constrained to lower levels (Figure 9(a)) and produced the near-surface lid seen in Figure 9(c). The higher lid (∼6 km in Figure 9(c)) prevents the release of the potential instability through a deep layer. This lid is seen as a stable and warm layer at ∼475 mb in Figure 9(d). The strength and depth of the upper-level lid decreases toward the northeast (Figure 9(c), cf. Figure 9(d) and (e)).

The exact location where convection initiated in relation to the terrain, as well as the life cycle of the system, is shown in Figure 11. Convection formed at 1900 UTC (0000 LST) over the easternmost edge of a relatively small ridge at ∼72°E, 33.8°N (thick solid contour in Figure 11(a)). The area of intense rainfall increased by 2000 UTC (short dashed contour). In the subsequent 2–3 hours the system moved toward the east-southeast (long dashed and thin solid contours, respectively). A vertical cross-section along the north–south line in Figure 11(a) indicates that the convection first appeared over a relatively small (<0.5 km) but sharp peak of the terrain (at distance = 270 km in Figure 11(b)).

Therefore the air column just upstream of the ridge, depicted in Figure 9(e), was subjected to 0.5 km (∼50 mb) of lifting. The sounding in Figure 9(f) shows the stratification resulting from subjecting the sounding in Figure 9(e) to ∼50 mb of lifting. The main layer that experiences destabilization is in the mid-levels (750–450 mb); however the near-surface air is also destabilized. A cross-section along the location where the convection started (yellow line in Figure 8(f)) reveals that there is a strong updraught breaking through the thin low-level lid and through the edge of the deeper upper lid (Figure 12(a)–(b)). The convection did not erupt over peaks farther to the south (e.g. at distance = 110 km in Figure 11(b)) because at this location the flow was farther from saturation and the orographic lifting was not enough to release the potential instability.

This analysis shows that orographic lifting is the triggering mechanism for the convection. A small but abrupt amount of uplift, provided by a steep foothill, was sufficient to remove both the lower and upper capping layers. An indirect implication of this result is that neither synoptic-scale lifting associated with the monsoon low, nor upward motion driven by the contrast in sensible heating between the Thar Desert and adjacent regions were likely strong enough to release the existing potential instability. Therefore, the potential instability was able to increase as a result of the persistent surface heat fluxes until the time of release. These results not only confirm the suggestion of H07 that foothill orography is crucial to the release of the instability but also add further insight by showing that the orographic lifting removes

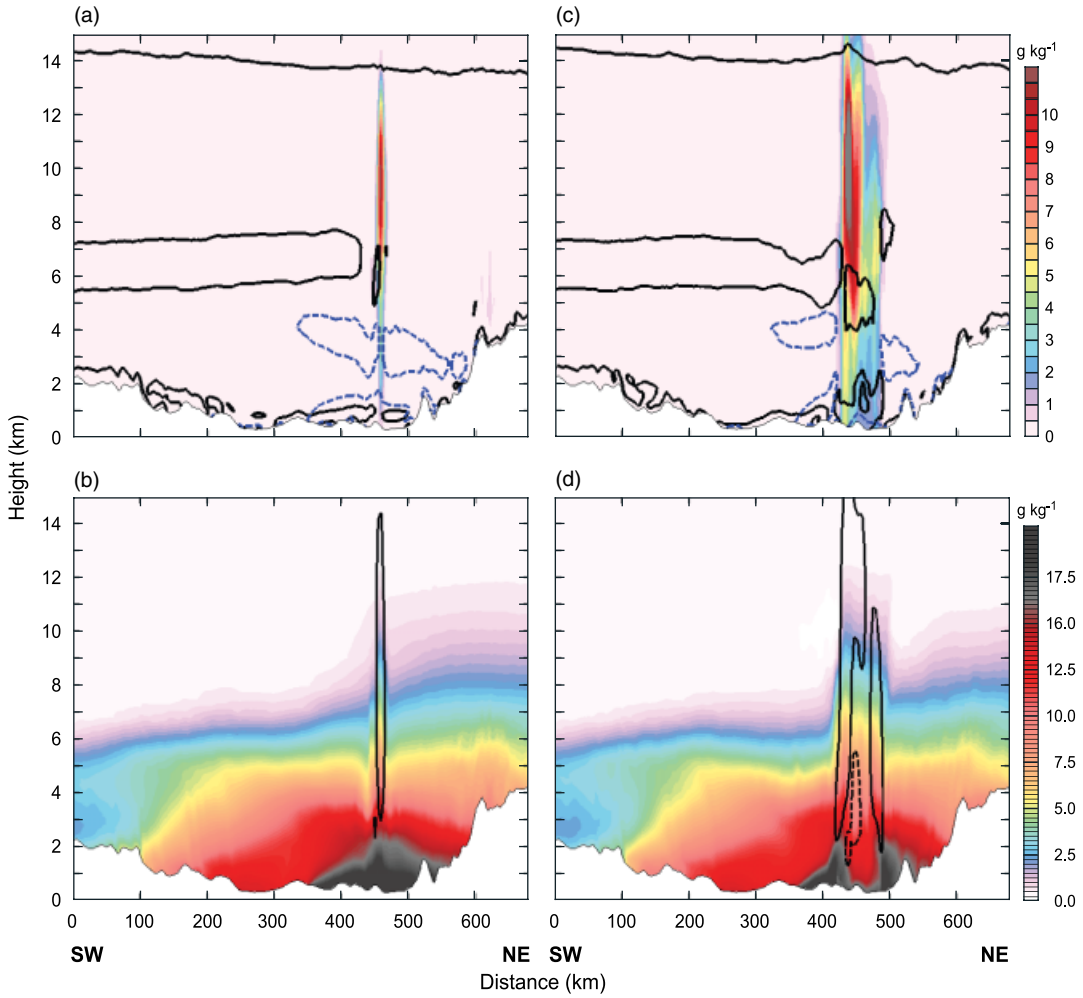

Figure 12. Vertical cross-section along the yellow line in Figure 8(f) of simulated variables during a *system containing intense convective echoes* at (a)–(b) the time of convection initiation (1900 UTC 3 September 2003) and (c)–(d) 2015 UTC 3 September. Panels (a) and (c) show total precipitation mixing ratio (colour shading), $d\theta/dz$ (black contour, 6 K km^{-1} isoline) and $d\theta_e/dz$ (blue contour, -6 K km^{-1} isoline). Panels (b) and (d) show water vapour mixing ratio (colour shading) and vertical velocity (solid and dashed contours indicate the 2 and -2 m s^{-1} isolines, respectively). The underlying terrain is shown by white fill. All fields are from Domain 2. [Correction made here after initial online publication.]

both the lower and upper stable layers, allowing extreme convection to occur.

5.6. *Upward motion and hydrometeors*

H07 suggested that the high values of reflectivity detected by the TRMM PR in the upper levels of the troposphere were the result of graupel particles being lofted to high altitudes by extremely strong updraughts. Figure 13 depicts vertical cross-sections along the northwest–southeast line in Figure 11(a) at the initial (1915 UTC) and mature (2130 UTC) stages of the system's life cycle. Initially, relatively isolated, deep, and erect reflectivity echoes, associated with very strong upward motions (>20 m s^{-1}) appeared over a small peak in the terrain (Figure 13(a)). The precipitation consisted of large amounts of graupel with some snow above the 0°C level and rain below (Figure 13(b)). As was suggested by H07, the 1 g kg^{-1} contour of graupel extended as high as 16 km, near the tropopause (~17 km at this time of the year). As the system aged, updraughts and convective echoes were triggered at the leading edge of the system and they maintained their vertically erect structure (Figure 13(c)). The trailing portion of the system was composed of older convective cells and stratiform precipitation, which exhibited a bright band (Figure 13(c)). This development of stratiform precipitation by the weakening of previously intense cells follows the process suggested by Houze (1997). During the mature stage, the concentrations of rain and graupel decreased compared to the initial stage; however, the region of occurrence of snow and graupel was more extensive than before (Figure 13(d)).

Another important water species to consider is water vapour. Figure 12(c) and (d) show a vertical cross-section through the system 2.25 hours after convection initiation. The area where the precipitation is stronger (Figure 12(c)) is also the region where high water vapour content air is being transported as high as 12 km by strong updraughts (Figure 12(d)). Therefore, the *system containing intense convective echo* of 3 September 2003 transported moisture to mid- and upper levels. This fact, as well as the analysis of satellite data, suggests that the mid- and upper level moisture seen before convection initiation (Figure 9(a)) may have been produced by a previous convective system. This is consistent with the results of H07 and Romatschke *et al.* (2010), who found frequent convection in this region during the monsoon (circle in Figure 1). These results suggest that the moistening of the mid and upper atmosphere by a previous but no longer active convective system may be an

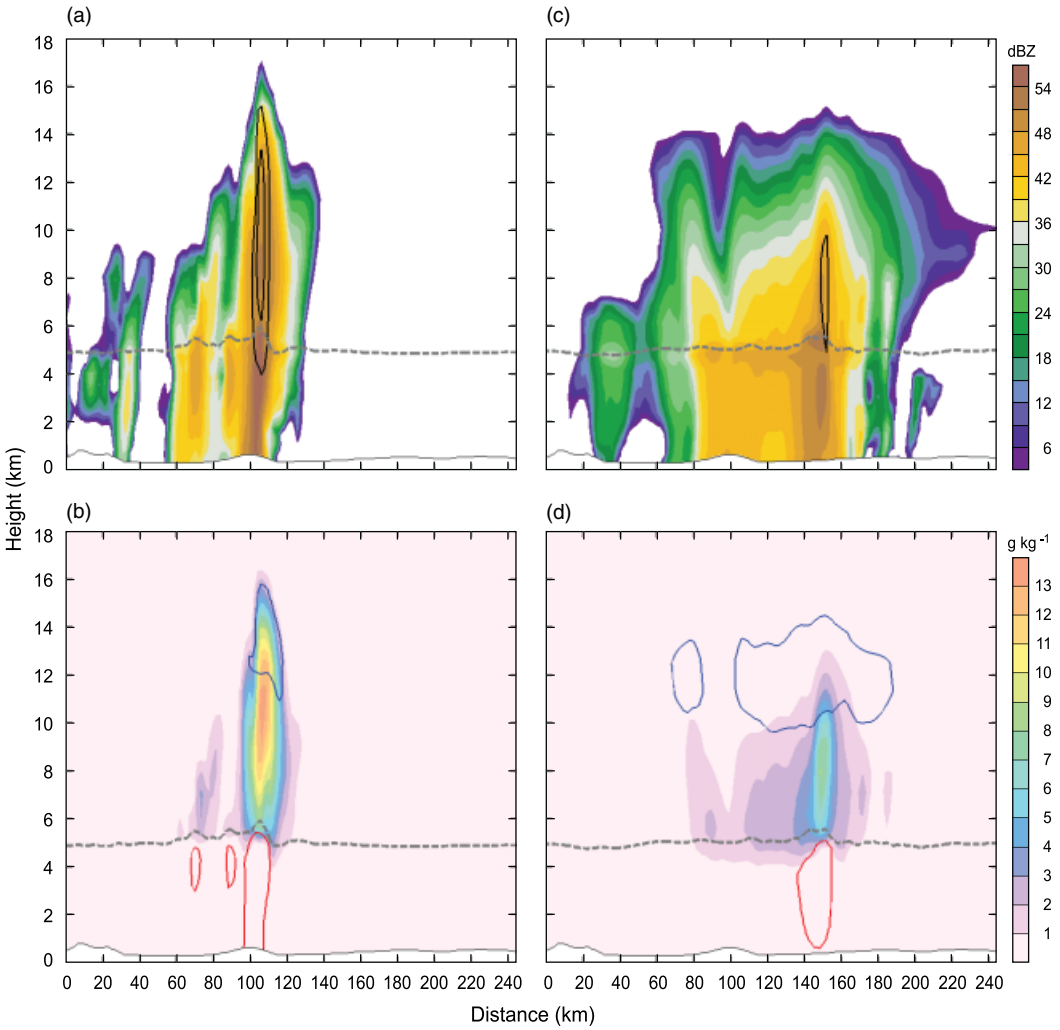

Figure 13. Simulated variables during a *system containing intense convective echoes*. Vertical cross-section along the northwest–southeast-oriented line in Figure 11(a) showing in the top row reflectivity and updraught velocity (black contours, 10 m s^{-1} intervals) and in the bottom row precipitating hydrometeors: graupel (colour shaded), snow (blue contour, 0.5 g kg^{-1} isoline), and rain (red contour, 2.0 g kg^{-1} isoline). The grey dashed line shows the 0°C level. (a)–(b) At 1915 UTC and (c)–(d) 2130 UTC 3 September 2003. The underlying terrain is shown in white fill. All fields are from Domain 2.

important ingredient in pre-conditioning the atmosphere for an intense precipitation event.

6. A typical example of a convective *system containing broad stratiform echo* in the northeastern subcontinent

6.1. Simulation details

The TRMM-PR-derived climatological database of H07 and Romatschke *et al.* (2010) shows that convective *systems containing broad stratiform echo* (>50 000 km^2) occur frequently near the eastern Himalayan foothills. We have chosen a typical example of such a system to simulate. This event occurred on 11 August 2002. The model orography and accumulated precipitation throughout the simulation are shown in Figure 14. This system was simulated for three domains (Figure 14). The simulation for Domain 1 has 27 km horizontal resolution and is used to evaluate whether the model is able to capture the synoptic features associated with this event. It was conducted independently of the other two domains. Domain 2 has 9 km resolution and nested within it is Domain 3, which has 3 km resolution. The simulations for Domains 2 and 3 were conducted with two-way nesting. The simulations started at 1200 UTC 10 August 2002 and lasted for 15 h; hence, the simulation was for the period from 1800 LST[††] 10 August to 0900 LST 11 August 2002, depicting the evening-to-morning evolution of this long-lasting event.

6.2. Simulation evaluation

The 10 m winds from the NCMRWF reanalysis are compared with the simulated surface winds at 0000 UTC 11 August 2002 (Figure 15). The model captured the Bay of Bengal depression observed near the western border between India and Bangladesh. The wind direction is well captured by the model simulation, while the wind speed is slightly overestimated over the Indian Peninsula and the Bay of Bengal. At Tengchong ('T' in Figure 15(b)), the simulated sounding at 0000 UTC 11 August 2002 (Figure 16(b)) captured the saturated, moist-adiabatic atmospheric conditions observed at this time (Figure 16(a)). Farther upstream, at Kolkata ('K' in Figure 15(b)), the model

[††]This event extended over several countries but was loosely centred over Bangladesh. Therefore we will reference this event with the LST of Bangladesh, which is UTC + 0600.

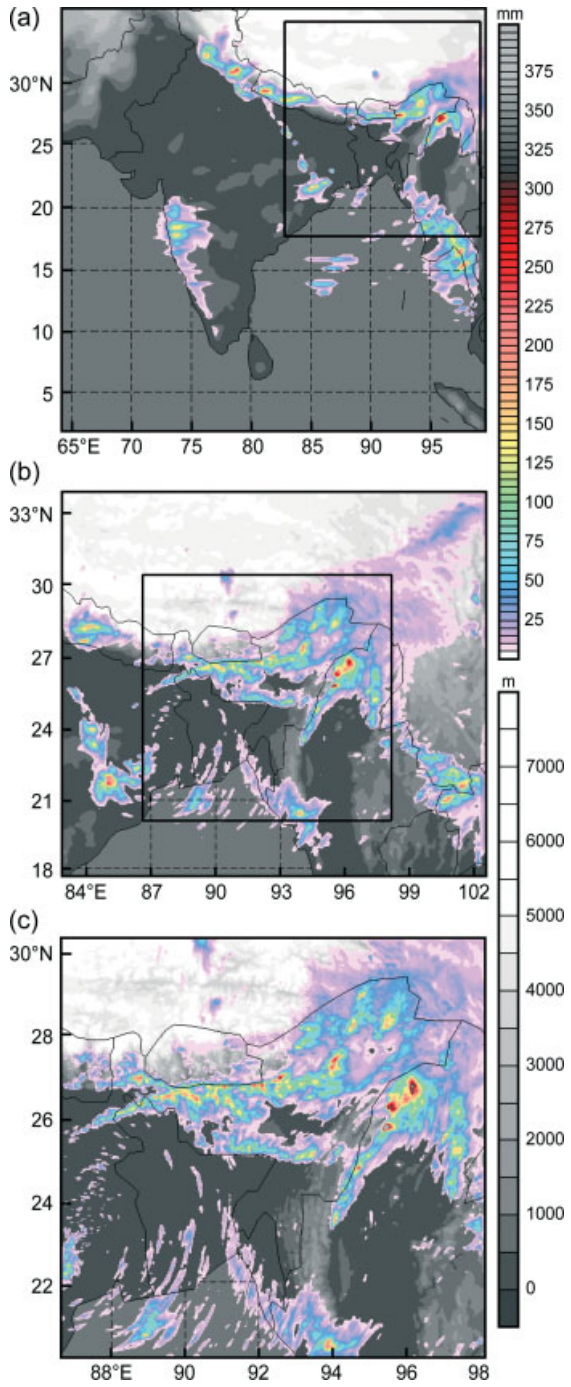

Figure 14. Domains used to simulate a convective *system containing broad stratiform echo*. The terrain (grey shading) and accumulated precipitation (colour shading) throughout the simulation (1200 UTC 10 August to 0300 UTC 11 August 2002 (1800–0900 LST 11 August 2002)) are shown for (a) Domain 1 (horizontal resolution = 27 km), (b) Domain 2 (horizontal resolution = 9 km), and (c) Domain 3 (horizontal resolution = 3 km).

also captured the observed conditions (Figure 16(c)–(d)). The available instantaneous view of TRMM-PR reflectivity indicates that the model was able to accurately simulate the location of the precipitating system on the eastern indentation of the Himalayas (Figure 17). The observed and simulated reflectivity values are comparable (Figure 17(a) and (c)). A vertical cross-section through the simulated reflectivity field (along the black line in Figure 17(c)) reveals upright convective echoes surrounded by a horizontal bright-band echo (Figure 17(d)), in agreement with the observations (Figure 17(b)). The simulated echo tops are higher than in the observations; however, there are a few issues that complicate making quantitatively accurate observed–simulated reflectivity comparisons: first, the simulated echoes above ∼8 km would be undetectable by the TRMM PR 17 dBZ sensitivity threshold, and second, the model's simulation of radar reflectivity is based on simple assumptions that may not be realistic enough.

Since the system was in general terms well captured by the simulation, the model output will be used, along with NCEP data, to test the hypotheses put forward by H07. The source of the information used (i.e. observations or simulation), is clearly indicated in each figure caption.

6.3. *Airflow origin and moisture sources*

H07 suggested that as the low-level flow passes over the Bay of Bengal and the Bangladesh wetlands, these areas provide an important source of moisture for the rainfall systems observed near the Himalayas during convective *systems containing broad stratiform echoes*. This section analyses the airflow origin and the moisture sources for the simulated case.

Since the WRF simulation does not extend far enough in time, we use HYSPLIT backward trajectories to assess the origin of the flow that reached the Himalayan foothills at 0000 UTC 11 August 2002. The trajectories ending at 0.5 and 6.0 km AGL (black and white trajectories in Figure 18(a), respectively) illustrate that the air parcels in the whole lower troposphere resided over the Bay of Bengal up to ∼3 days before reaching the end points. Thus, a deep layer advanced from the moist Bay of Bengal toward the Himalayan foothills. The characteristics of the low-level parcels are shown in Figure 18(b)–(d). The air temperature of the parcels as they moved over the Bay of Bengal was fairly constant, while the water vapour mixing ratio and θ_e increased. As the trajectories reached the Bangladesh wetlands (denoted by the white square in Figure 18(a)), the meteorological variables were subjected to some diurnal variability (solid symbols in Figure 18(b)–(d)). However, the parcels spent ∼21 h over the Bangladesh region, making the time of the day at which they arrive at the Bangladesh region irrelevant, as they will experience nearly a full diurnal cycle here. The maximum mixing ratio and θ_e values attained over the wetlands are as large, if not larger, as those attained over the Bay (Figure 18(c)–(d)).

The NCEP reanalysis surface fluxes of heat in the days preceding the event are analysed over the Bay of Bengal (17.5–21°N, 88–92°E) and over Bangladesh (21.5–25°N, 88–92°E), regions indicated by the large squares in Figure 18(a). The following discussion is based on Figure 19. Over the Bay, the latent heat flux dominates over the sensible heat flux, which is very small (dashed lines with circles and crosses). Over Bangladesh, the surface fluxes of latent and sensible heat have a strong diurnal cycle (solid lines with circles and crosses, respectively), with the surface flux of latent heat dominating, particularly between 0000–1200 UTC (0600–1800 LST) when it may reach ∼250 W m^{-2}. Therefore, depending on the time of the day, both the Bangladesh wetlands and the Bay of Bengal may have significant surface fluxes of latent heat. Hence, the Bay of Bengal and the Bangladesh wetlands are both important sources of moisture to the eastern Himalaya indentation.

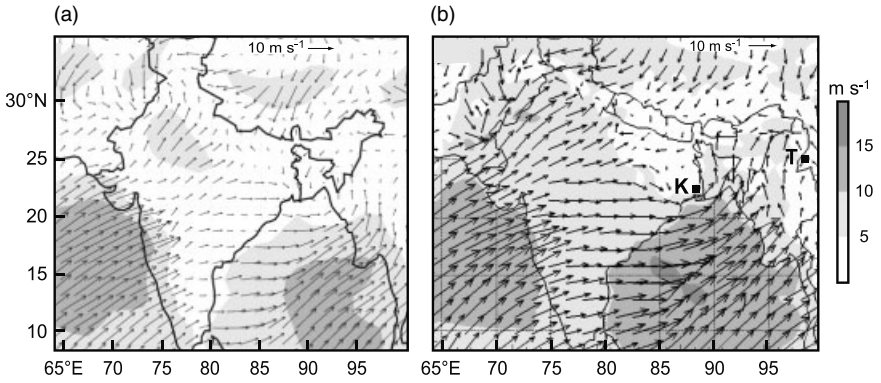

Figure 15. (a) NCMRWF reanalysis 10 m winds and wind speed and (b) simulated (from Domain 1) surface winds and wind speed for a convective *system containing broad stratiform echo* (0000 UTC 11 August 2002). The location of sounding stations are indicated in (b) by T (Tengchong) and K (Kolkata).

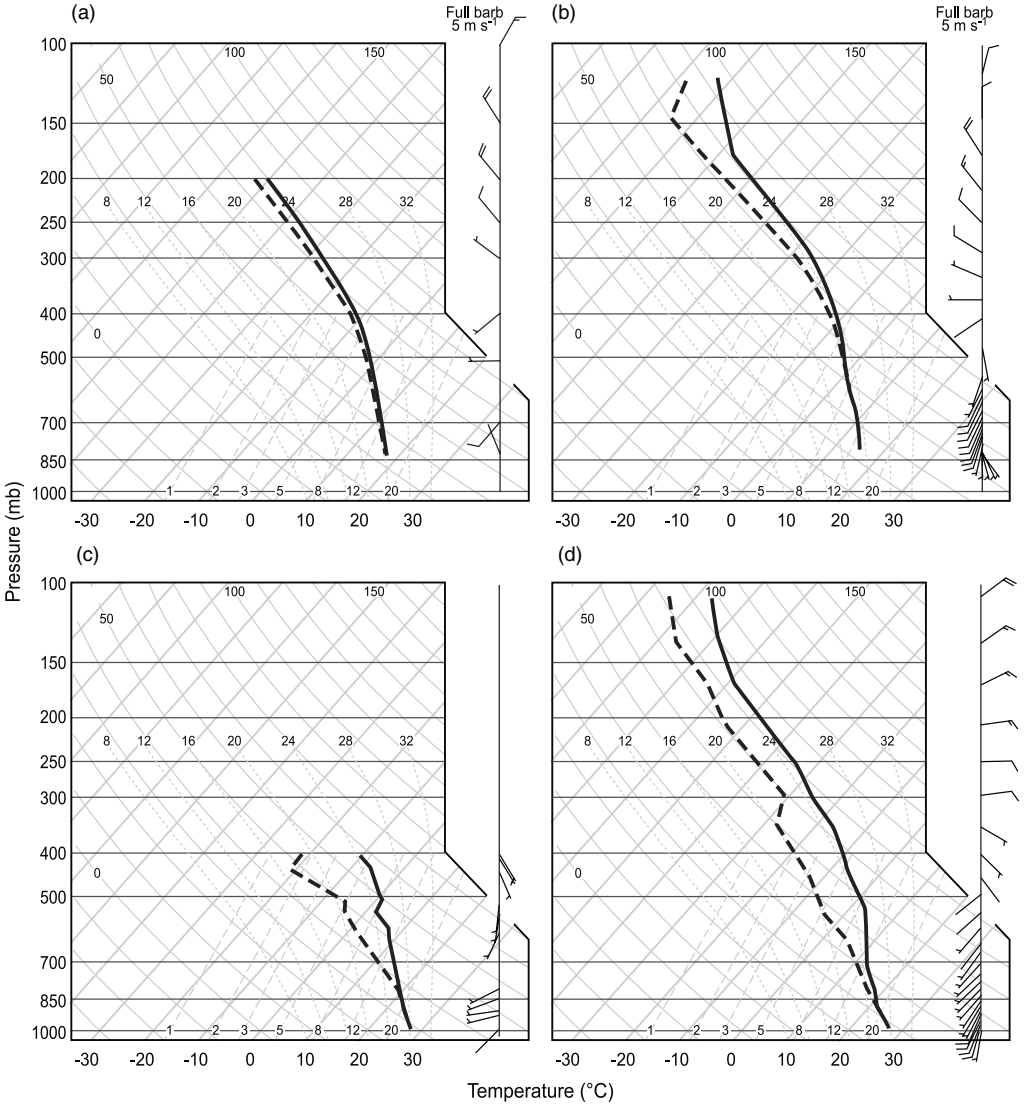

Figure 16. Observed (first column) and simulated (Domain 1, second column) soundings for a convective *system containing broad stratiform echo* at (a)–(b) Tengchong and (c)–(d) Kolkata at 0000 UTC 11 August 2002. The locations of the soundings are shown in Figure 15.

The grey bar in Figure 19 indicates the time period of the WRF simulation, which corresponds to a minimum in the latent heat surface flux over Bangladesh. The following discussion is based on Figure 20(a), which shows model output averaged (accumulated in the case of the precipitation) during the full length of the simulation. The white contour in Figure 20(a) shows the 200 W m^{-2} isoline of surface flux of latent heat. During the averaged period, which did not include the land diurnal maximum (Figure 19), the surface flux of latent heat was maximum over the Bay of Bengal and Arabian Sea, in regions where the surface wind speed was large (black contours). The surface wind speed was apparently stronger than the climatology (Figure 3(a)) over the oceans and low-elevation land. The

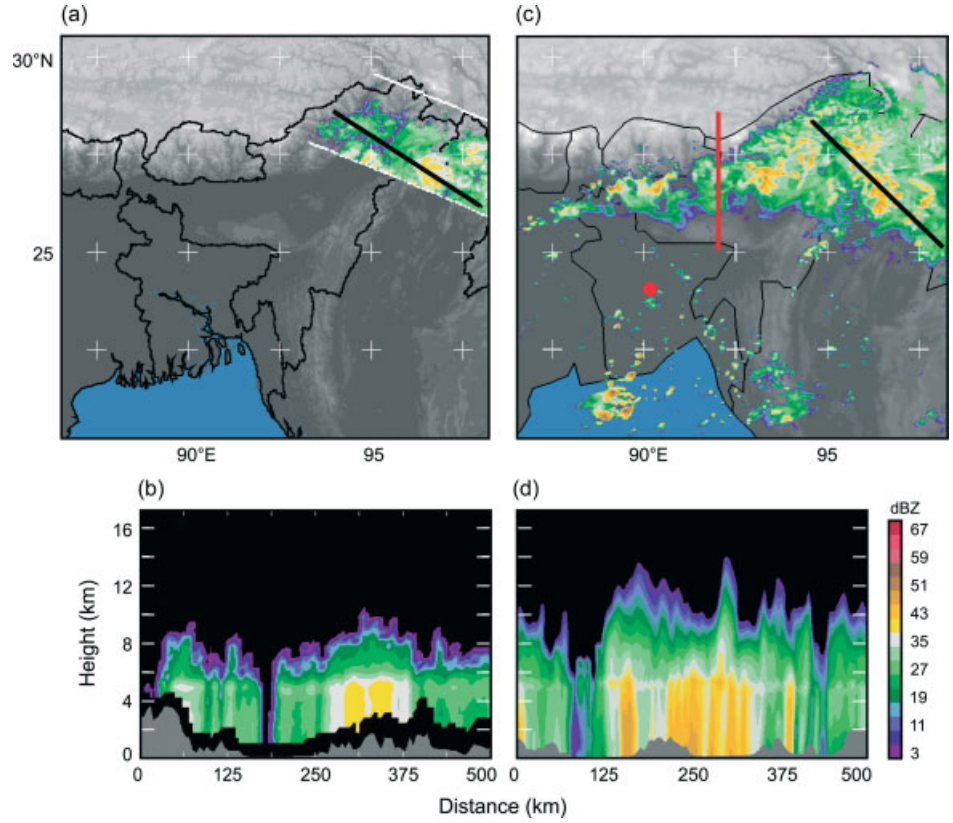

Figure 17. (a)–(b) TRMM observed and (c)–(d) simulated (Domain 3) reflectivity for a convective *system containing broad stratiform echo* at 0253 UTC 11 August 2002 (observation) and 0245 UTC 11 Aug 2002 (simulation). Panels (a) and (c) show horizontal cross-sections at 4 km. Panels (b) and (d) shown vertical cross-sections taken along the black lines in panels (a) and (c), respectively. The red line and circle in (c) indicate the location of the cross-sections and soundings discussed in the text. Observed panels adapted from Houze *et al.* (2007).

strong southwesterly low-level winds over the Bay of Bengal and the Arabian Sea likely aided in the extraction of moisture from the ocean by wind-induced surface heat exchange (Emanuel, 1986, 1987; Yano and Emanuel, 1991; Emanuel *et al.*, 1994). The precipitable water (blue contour) became maximum downstream of the area of maximum wind speed and surface flux of latent heat, suggesting that the moisture derived from the ocean was advected into the region of the subcontinent by persistent southwesterly monsoonal flow from the Bay of Bengal and Arabian Sea[‡‡]. The moist air was accumulated upstream of the south- and west-facing mountain ranges (Himalayas, Bilauktaung and western Ghats), attaining moisture content higher than the season climatology (Figure 3(a)). Hence there was anomalously large cross-barrier moisture flux during this event. The moist air was preferentially converted into precipitation over the foothills of the terrain (red contours), which strongly suggests that orographic rather than synoptic lifting was the cause of the precipitation. The precipitation mechanism will be discussed in detail in the next two sections.

6.4. *Triggering of convective precipitating cells*

The nature of the TRMM-observed reflectivity (Figure 17(a)–(b)), which consists of a bright-band echo with embedded convective echoes, led H07 to hypothesize that the stratiform echo was formed by dying convective cells, a process described by Houze (1997). The analysis of Rafiuddin *et al.* (2010) of ground-based radar data over Bangladesh, a region where convective *systems containing broad stratiform echo* are frequently observed during the monsoon, suggests that this may be the case. They found that the convection in this season and region is characterized by MCSs that on occasion are so large that they completely cover the radar's domain (∼400 km range). Rafiuddin *et al.* (2010) called these systems 'scattered-type with wide area coverage' (SWAC). The time continuity provided by the ground-based scanning radar showed that within these systems small echoes grow and disappear continuously. However, neither H07 nor Rafiuddin *et al.* (2010) had the detailed dataset necessary to understand the mechanisms controlling the evolution of these systems. In this section, we analyse the evolution of a simulated convective *system containing broad stratiform echo* to address this point.

Two periods illustrative of the initial and mature stages of the simulated system are presented in Figure 21. These vertical cross-sections were extracted along the red line in Figure 17(c). Figure 22 shows soundings corresponding to the initial and mature stages at the location indicated by the red circle in Figure 17(c). The precipitation at the initial stage consisted of deep, narrow cells with echo tops reaching ∼13 km. These cells formed as conditionally unstable and slightly sub-saturated south-southeasterly flow below 650 mb (Figure 22(a)) reached the Khasi Hills and the lower Himalayan foothills (Figure 1), where it was orographically lifted to saturation, causing it to become statically unstable (Figure 21(a)). The updraughts associated

[‡‡]The surface flux of latent heat from the Bangladesh wetlands was evidently also important (Figure 19); however, the simulation does not extend long enough to capture the time when this effect was at its maximum.

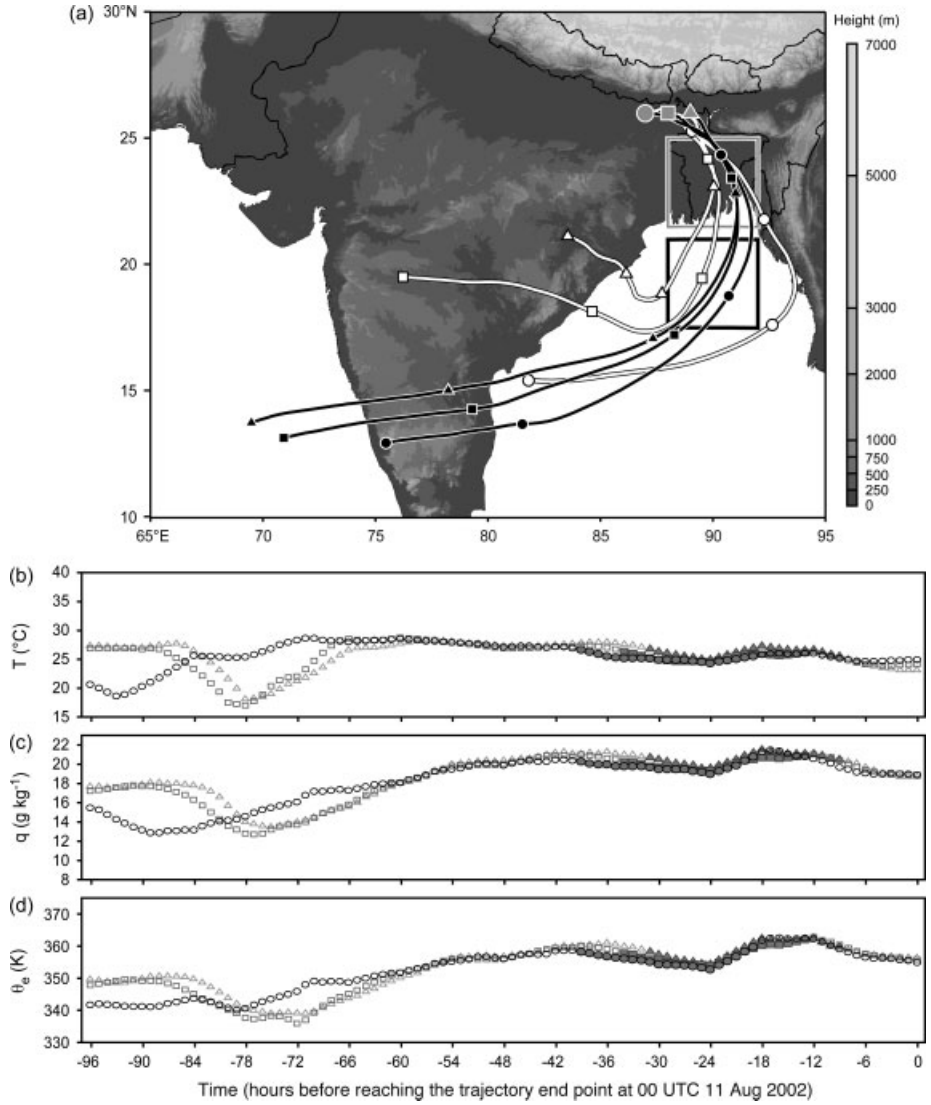

Figure 18. As in Figure 7 but for trajectories coinciding with the occurrence of a convective *system containing broad stratiform echo.* (a) Trajectories for parcels reaching the locations indicated by the grey symbols at 0000 UTC 11 August 2002 at 6.0 km AGL (white trajectories) and 0.5 km AGL (black trajectories). The large squares identify the regions over the Bay of Bengal and Bangladesh used in Figure 19. (b)–(d) Time series for the low-level trajectories shown in (a). The solid symbols identify the period when the low-level trajectories were over Bangladesh.

with the convective cells were >1 m s^{-1} (Figure 21(a)). The precipitating hydrometeors in the cells consisted of large amounts of graupel with some snow above the 0°C level and rain below (Figure 21(b)).

As the system aged, the updraughts decreased in intensity, the echoes became shallower, and they took on a stratiform character with embedded convection (Figure 21(c)). The flow retained some low-level instability, as can be seen in the 950–850 mb saturated and unstable layer in Figure 22(b). Therefore, additional convective cells were released within the otherwise stratiform rain region. As the convective system transitioned from the initial to the mature stage, the amount of graupel decreased sharply but the horizontal extent of the snow and rain increased (Figure 21(d)).

After the initial stage, the triggering of new cells was not exclusively over the foothills. Zooming in over a small area between the Himalayan foothills and the Khasi Hills (Figure 1) reveals that the generation of new convective precipitation was very complex during this event. The convective cores that were initially triggered at the Himalayan foothills (e.g. Figure 21(a)) began to grow, merge, and develop cold pools, which started moving away from the foothills and toward the plains – probably as a gravity-driven drainage flow (Figure 23). New convective cells were later triggered over the plains between the Himalayas and the Khasi Hills (not shown) as the cold-pool flow converged with either other cold pools from cells triggered farther upstream, with downslope flow on the lee of the Khasi Hills or with the large-scale monsoonal flow.

We suspect that similar mechanisms and precipitation evolution occur over the eastern portions of the Arabian Sea and the Bay of Bengal, where convection is often triggered upstream of the western Ghats and the coastal mountains of Burma (Grossman and Durran, 1984; Xie *et al.*, 2006). We speculate that in these regions the precipitation is initially triggered over the coastal terrain as deep convective echoes. These convective cells may produce upstream-propagating cold-pool flows that upon encountering the moist and southwesterly monsoonal flow induce convergence and triggering of convection upstream of the mountains. Then, as these echoes age and weaken, they transition into a stratiform system with embedded convection that is advected downstream, where it is subjected to gentle orographic lifting over the coastal

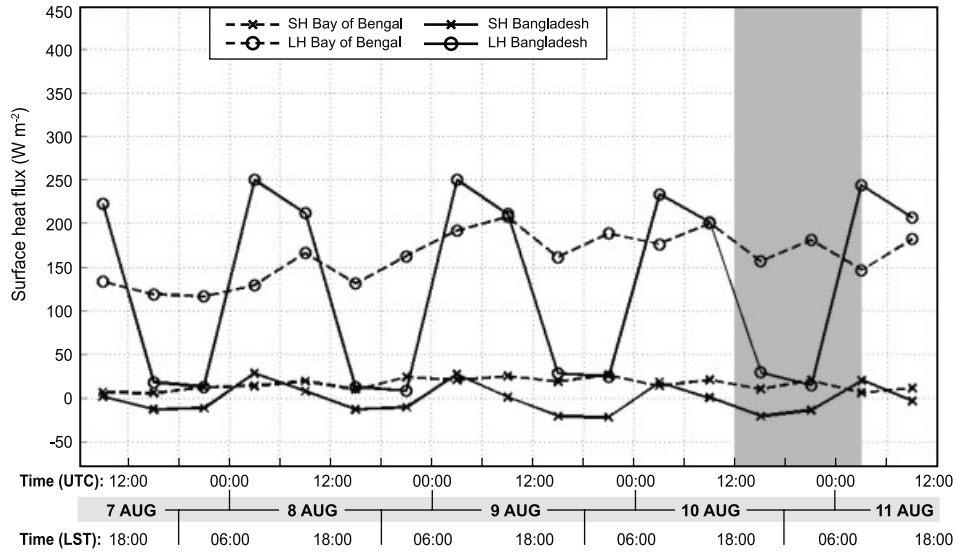

Figure 19. As in Figure 10 but for the days leading up to a convective *system containing broad stratiform echoes*. The fluxes were averaged over the Bay of Bengal (dashed lines) and over Bangladesh (solid lines). The location of these regions is indicated by the large squares in Figure 18(a).

terrain, reinforcing the stratiform precipitation. Grossman and Durran (1984) suggested that the upstream triggering resulted from blocking of the low-level flow; however, further studies are needed to investigate this new hypothesis.

The results outlined in this section have many similarities to the findings of Nuissier *et al.* (2008) and Ducrocq *et al.* (2008), who used mesoscale simulations to study convection over the coastal terrain of southern France. They found that the convection occurred as a result of a combination of synoptic and fine-scale processes. In particular, they found that the oceanic surface provided an important moisture source and that the convection was triggered in some cases over the fine-scale terrain and in others upstream of the terrain over the leading edge of a cold pool produced by another system.

6.5. *Orographic enhancement of stratiform precipitation*

H07 hypothesized that as the stratiform mesoscale precipitation areas associated with convective systems embedded within Bay of Bengal depressions encounter the eastern indentation of the Himalayas, the stratiform rainfall is enhanced by orographic lifting. In this subsection we examine the consistency of this hypothesis and illustrate the ways in which synoptic and orographic lifting affect the convective systems in this region.

In the previous section we saw that the initial stage of the event consisted of convective cells that were triggered over and upstream of the lower foothills. As the system aged, the echoes became shallower and stratiform with embedded convection. Animation of the simulation output (available at http://www.atmos.washington.edu/~socorro/PAPER_SUPPLEMENT/BROAD_ECHO_loop.gif) reveals that as each new set of convective cells became more stratiform, they were advected downstream toward the north or northeast, farther into the eastern indentation of the terrain, where the air containing them could be subjected to gentle orographic lifting. To illustrate and quantify this process, we refer to the model fields averaged throughout the simulation (Figure 20). Except for the southwest quadrant of the depression, there was little precipitation near the centre of the low-pressure system (red contours in Figure 20(a)–(b)) and little upward motion (orange contours in Figure 20(b)). Therefore, the synoptic depression did not provide much lifting. As will be shown below, its role was to provide persistent southwesterly moist flow, which subsequently impinged upon the terrain and was subjected to orographic lifting.

The maximum accumulated precipitation throughout the simulation occurred over the Western Ghats, the Bilauktaung range and the Himalayan foothills (red contours in Figure 20(a)). These areas were exposed to strong and moist cross-barrier winds. We will focus on the precipitation maximum near the eastern Himalayas. Throughout the simulation, the synoptic-scale surface low-pressure system (white contours in Figure 20(b)) was nearly stationary and centred near the western border of Bangladesh and India. The region of low pressure coincided with the area of high precipitable water (blue contour in Figure 20(b)). The mean circulation associated with the depression brought moist air from the Bay of Bengal and the Bangladesh wetlands toward the low-lying areas in the eastern indentation of the Himalayas. The moist air was preferentially converted into precipitation when the low-level flow reached the lower foothills of the terrain (red contours in Figure 20(b)). The regions of maximum accumulated precipitation coincide with areas of mean upward motion at 500 mb over the Himalayan slopes (orange contours in Figure 20(b)), indicating that the precipitation was formed as the low-level flow was lifted over the terrain.

A vertical cross-section along the yellow line in Figure 20(b) shows that the airflow in the direction parallel to the cross-section was toward the mountains below ~8 km and that it had a low-level jet that rose over the terrain (Figure 20(c)). This structure is similar to that observed during several Mesoscale Alpine Program (MAP: Bougeault *et al.*, 2001) Intensive Observing Periods (IOPs) (e.g. IOP 2b, 3 and 5), when slightly conditionally unstable near-saturated air originating over the Mediterranean Sea rose in the form of an upslope low-level jet over the windward Alpine slopes (Medina and Houze, 2003; Rotunno and Houze, 2007). The air reaching the eastern indentation of the Himalayas was nearly saturated and close to moist adiabatic (Figures 16(b) and 22(a)). The terrain channelled the low-level air and concentrated it into a low-level jet. Because of the low moist

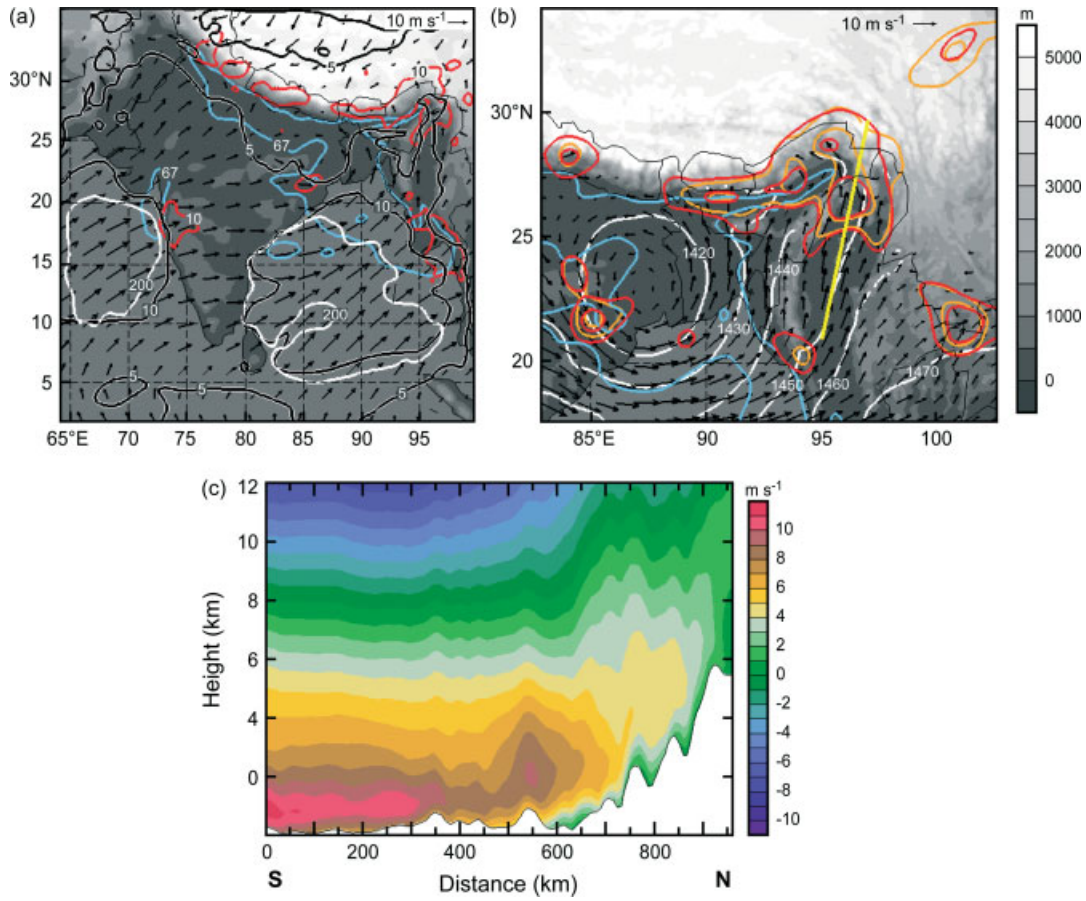

Figure 20. Time-averaged fields during the simulation of a convective *system containing broad stratiform echo*. (a) Surface wind vectors and speed (m s^{-1}, black contours), surface flux of latent heat (white contour), precipitable water (blue contour), and accumulated precipitation (red contour). (b) 850 mb winds and geopotential heights (white contours), precipitable water (blue contour, 67 mm isoline), 500 mb vertical velocity (orange contours, 0.05 m s^{-1} intervals), and accumulated precipitation (red contours, 20 and 50 mm isolines). (c) Vertical cross-section (averaged along the yellow line in (b) ±5 grid points) of airflow in the direction parallel to the cross-section. Positive values denote flow from left to right. The terrain is shown in grey shading in (a)–(b) and in white fill in (c). The fields in panel (a) are from Domain 1, while in panels (b)–(c) they are from Domain 2. All fields were smoothed.

static stability, the low-level jet rose easily over the slopes. The moisture-laden low-level jet transported moisture over the windward slopes, where it was condensed into cloud water, which could be collected by falling precipitation. This process enhanced the stratiform precipitation and contributed to the formation of an extremely large stratiform rain area over the eastern terrain (Figure 17). Thus, the tendency of the convection to evolve into large stratiform precipitation regions is synergistic with the upslope flow, accounting for the maximum of precipitation along the lower windward slopes of the Himalayas.

7. Conditions leading to regional differences in convective structures

During the monsoon, precipitating *systems containing intense convective echoes* occur frequently in the western Himalayan indentation (circle in Figure 1), while on the eastern side (black solid rectangle in Figure 1) convective *systems containing broad stratiform echo* dominate (H07; Romatschke *et al.*, 2010). Typical cases of each type of system were studied in sections 5 and 6. In this section, we compare the climatological conditions of the monsoon season with those observed during our case-studies to assess their representativeness.

Important factors for the western Himalayan *system containing intense convective echoes* of 3 September 2003 included: surface moisture flux from the Arabian Sea, surface flux of sensible heat from the Thar Desert, and moisture flux from the western terrain indentation (section 5.4). The discussion for the rest of this paragraph is based on Figure 24(a), which shows the monsoon climatological diurnal cycle of the surface fluxes over these regions (squares in Figure 7(a)). Over the Arabian Sea, the surface latent heat flux dominates and is ∼100 W m^{-2} at all times (dashed line with circles). In contrast, the fluxes over land have a strong diurnal cycle characterized by high values during the daytime. While over the dry and barren Thar Desert the surface flux of sensible heat (solid line with crosses) dominates during the daytime, the latent heat is the dominant flux over the western indentation (dotted line with circles). Therefore the climatological diurnal cycle of the heat fluxes are very similar to those observed in connection with the *system containing intense convective echo* of 3 September 2003 in the western subregion (Figure 10). These results suggest that the heat flux conditions observed during the case-study are in general representative of the average monsoonal conditions. One notable difference is that the surface flux of sensible heat in the western terrain indentation has more extreme variations in the climatology than in the case-study (cf. dotted line with crosses in Figures 24(a) and 10). This difference is understandable as this region only receives a moderate amount of precipitation during the monsoon (Figure 3(b)); therefore, in the days

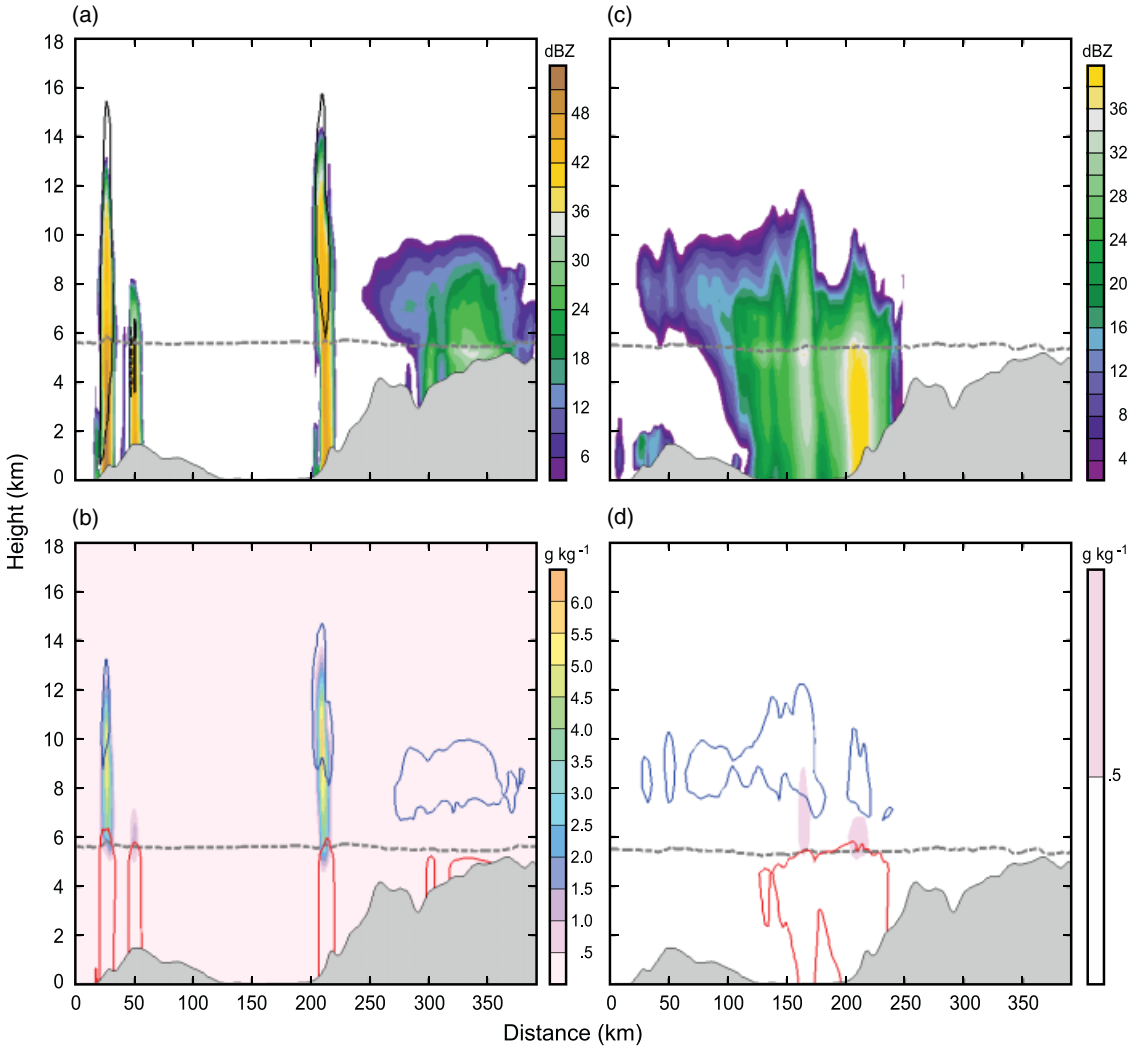

Figure 21. Simulated variables during a convective *system containing broad stratiform echoes*. Vertical cross-section along red line in Figure 17(c) showing in the top row reflectivity and updraught velocity (black contour, ± 1.0 m s^{-1} isoline with negative dashed) and in the bottom row precipitating hydrometeors: graupel (colour shaded), snow (blue contour, 0.1 g kg^{-1} isoline), and rain (red contour, 0.1 g kg^{-1} isoline). The grey dashed line shows the 0°C level. (a)–(b) At 1415 UTC 10 August, and (c)–(d) at 0130 UTC 11 August 2002. The underlying terrain is shown in grey shading. All fields are from Domain 3.

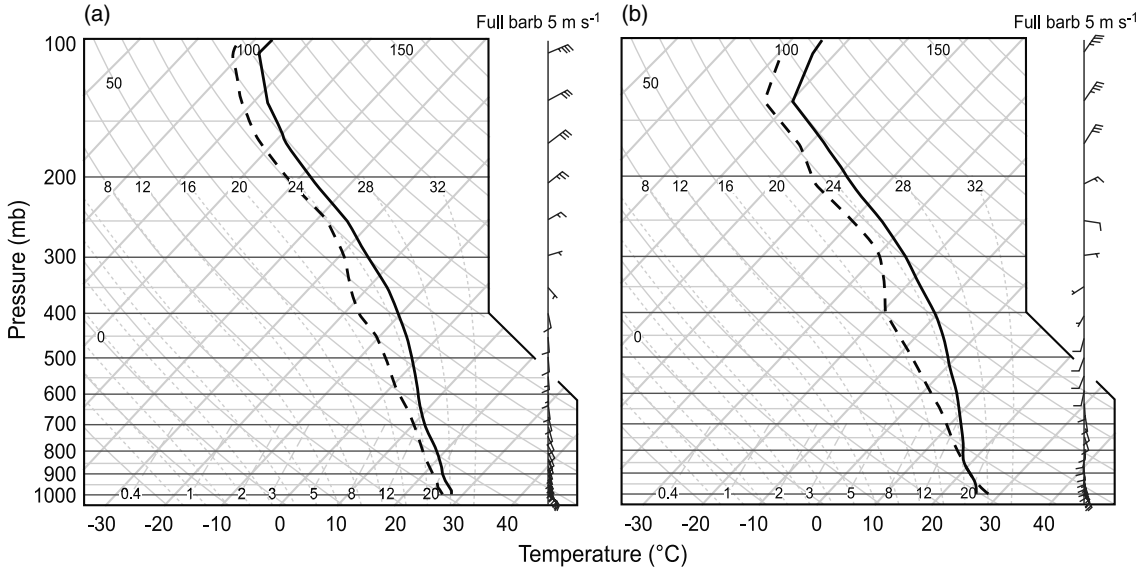

Figure 22. Simulated soundings for a convective *system containing broad stratiform echo* extracted upstream of Himalayas (24°N, 90.2°E, indicated by the red circle in Figure 17(c)) at (a) 1415 UTC 10 August and (b) 0130 UTC 11 August 2002. All fields are from Domain 3.

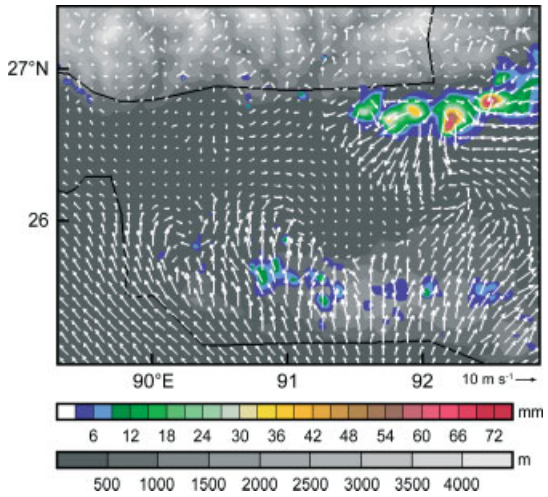

Figure 23. Zoomed detail of individual cells of a simulation of a convective *system containing broad stratiform echo* showing surface winds and vertically integrated mixing ratio of precipitating hydrometeors at 1745 UTC 10 August 2002. The terrain is shown in grey shading. All fields are from Domain 3.

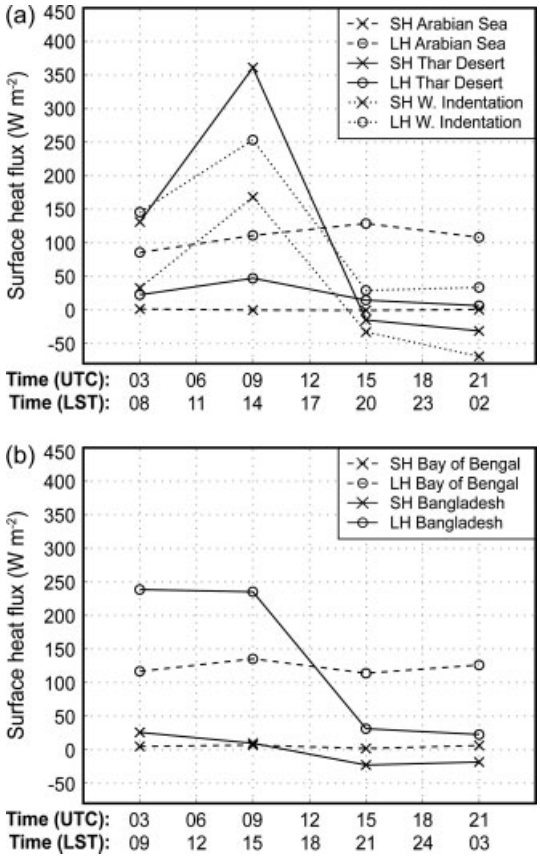

Figure 24. NCEP reanalysis mean diurnal cycle during the monsoon (June–September) of surface fluxes of sensible and latent heat (indicated by crosses and circles, respectively). The fluxes were averaged over the same domains used for (a) Figure 10, and (b) Figure 19.

when the soil is dry, the sensible heat flux likely increases. The other factors found to be important for the case-study are to a large degree associated with the general circulation and the terrain; hence they are also present during the monsoon season. For example, according to Bhowmik *et al.* (2008), large CIN over the Indus Valley and adjacent regions is a monsoon climatological feature. It appears that the precipitable water was anomalously high during the case-study (cf. Figures 3(a) and 7(a)). Thus, anomalously high precipitable water might be a useful parameter to consider in forecasting extreme precipitation in this region. The collection of factors outlined above may help explain why the western indentation is characterized by the frequent occurrence of *systems containing intense convective echoes*.

For the convective *system containing broad stratiform echo* of 11 August 2002 over the eastern Himalayan region, the surface moisture fluxes from the Bay of Bengal and over the Bangladesh wetlands were found to be important (section 6.3). The discussion for the rest of this paragraph is based on Figure 24(b), which shows the monsoon climatological diurnal cycle of the surface fluxes over these regions (squares in Figure 18(a)). Over the Bay of Bengal there is little diurnal variability and the surface latent heat flux ($\sim$120 W m^{-2}) dominates (dashed line with circles). Over the Bangladesh wetlands, the fluxes have a strong diurnal cycle characterized by a large daytime surface flux of latent heat $\sim$240 W m^{-2} (solid line with circles). Therefore the mean climatological diurnal cycle of the heat fluxes are very similar to those observed in association with the convective *system containing broad stratiform echo* case-study (Figure 19), suggesting that this case is representative of the average monsoon surface heat fluxes. Therefore, throughout the monsoon, the eastern side of the Himalayas has two reliable sources of boundary-layer moisture: the Bay of Bengal and the Bangladesh wetlands. With moisture continuously reaching the eastern indentation of the Himalaya, there is high potential for the precipitating systems in this area to grow very large, particularly considering that the moist flow is subjected to orographic lifting over the Himalayan foothills. As pointed out by Schumacher and Houze (2003), the development of large stratiform rain fractions, which are associated with tropical oceanic convection, is likely aided by near-moist-adiabatic stratification of the free atmosphere (Xu and Emanuel, 1989). Since the environment near the wetlands of Bangladesh has a maritime stratification of temperature and moisture, we suggest that this region is essentially a 'super-ocean', where the background moisture content of the maritime-origin air is fortified by diurnal pumping of moisture from the wetlands. In this respect, the Bangladesh region is similar to the Amazon region of South America. Additionally, in the presence of a Bay of Bengal depression, the large background monsoonal moisture flux is further increased near Bangladesh (cf. Figures 3(a) and 20(a)). Downstream there is enhanced southwesterly moist flow that is subjected to a strong orographic forcing over the Himalayas. We suggest that the facts outlined above may help explain why the eastern Himalayan region is populated by convective systems that develop extremely broad (>50 000 km^2) stratiform precipitation regions. When affected by Bay of Bengal disturbances, the region has ideal conditions for abundant precipitation. Not surprisingly, Cherrapunji, India, at the southern foothills of the Khasi Hills (25.2°N, 91.7°E), considered the wettest place on earth (Xie *et al.*, 2006), is located in this region.

8. Conclusions

Two case-studies, representative examples of extreme monsoon convection near the Himalayas, have been selected for this study. The environmental conditions that existed during the case-studies have many similarities with those

observed on average during the monsoon season. WRF model simulations have captured the essential features of a *system containing intense convective echoes* of the type that frequently occurs near the foothills of the western Himalayas and a typical convective *system containing broad stratiform echoes* of the type that is frequently observed near the eastern indentation of the Himalayas. The model simulations and available observations elucidate the roles of complex terrain, land–sea differences, and land-cover type in these two types of extreme summer monsoon convection. More specifically, these data have aided in testing, refining and quantifying the hypotheses of H07 regarding the formation of extreme convection in these regions. On the basis of these representative case-studies and of the analysis of monsoon climatological features, we can summarize the apparent key physical processes in these two types of extreme monsoonal convective systems as follows.

The *system containing intense convective echo* in the western Himalayan indentation is preceded by low-level monsoonal flow passing over the Arabian Sea, where it collects moisture via surface flux of latent heat. Upon making landfall, the surface flux of latent heat decreases, but the flux of sensible heat increases as the previously moistened low-level flow passes over the Thar Desert. Day after day, the surface flux of sensible heat over the Thar Desert exhibits a large diurnal cycle, reaching >300 W m^{-2} during the afternoon, which further increases the buoyancy of the already moisture-laden flow. As the low-level flow advances over the Himalayan foothills, it is exposed to large surface flux of latent heat, likely associated with evapotranspiration from soil moistened by earlier precipitating system(s). As a result, the flow that reaches the western concave indentation of the Himalayas has both high moisture content and a high degree of potential instability. The analysis conducted suggests that the terrain plays three main roles in modulating convection: (1) The west concave indentation of the barrier allows precipitable water and buoyancy to build up and reach values >50 mm and >3000 J kg^{-1}, respectively; (2) low-level and elevated layers of dry and warm air apparently cap the low-level monsoonal flow and prevent the release of convection upstream of the Himalayas; (3) the convection is triggered as the potentially unstable flow is lifted over a small peak of the foothills ($\sim$0.5 km). The low-level and elevated stable layers are removed by orographic lifting. The release of instability takes the form of intense convection, which has extremely strong updraughts (>20 m s^{-1}) that loft graupel to levels as high as 16 km. These interpretations are consistent with past analyses of monsoon convection in the region (Sawyer, 1947; Sivall, 1977). The meteorological, topographic and land-surface conditions outlined above are robust features observed throughout the monsoon and help explain the frequent formation of extremely deep convective cells in the western Himalayan region (Zipser *et al.*, 2006; H07; Romatschke *et al.*, 2010). The formation of intense convection in the western Himalaya region has parallels with the formation of severe convection east of the Rocky Mountains of the USA. However, in the latter case there is only one lid preventing the release of convection, whereas in the former case we have documented two lids located at different heights.

Convective *systems containing broad stratiform echo* typically occur near the eastern Himalayas in association with a Bay of Bengal depression. Such convective systems are generally favoured within the environment of the depression but appear to be accentuated on the east side of the depression, where the enhanced low-level southwesterly/southerly flow encounters mountainous topography not far from the coastline. The low-level flow extracts moisture from the Bay of Bengal through wind-induced surface heat exchange, as indicated by the high surface fluxes of latent heat over the Bay ($\sim$100–200 W m^{-2}). When the flow makes landfall and moves over the Bangladesh wetlands, additional moisture is extracted, especially in the morning and afternoon, when the surface flux of latent heat exceeds 200 W m^{-2} as a result of diurnal heating of the land. This study suggests that the terrain affects the convection in the following ways: (1) The eastern indentation of the terrain allows moisture to build up upstream of the Himalayas, resulting in precipitable water values >60 mm; (2) when the conditionally unstable low-level air reaches the lower foothills, it is orographically lifted to saturation, becomes unstable, and the instability is released in the form of narrow, vertically-oriented convective cells. These cells grow, merge, and produce cold-pool flows that propagate down the Himalayan slopes, where they converge with the prevailing southerly flow and trigger convection upstream of the Himalayas (mechanisms that may also be important in explaining the frequent convection observed upstream of the Western Ghats and Burma coastal ranges); (3) as the convective systems age, the echoes weaken, merge, and become more widespread and stratiform, while new convective cells continue to form, weaken, and merge into the stratiform regions. These convective systems with large stratiform regions are advected downstream farther into the eastern Himalayan indentation and over the Arakan Mountains. Since the maritime air within the stratiform precipitation regions is nearly saturated and neutral, it is easily lifted over the terrain as the strong cross-barrier flow characterized by a low-level jet impinges on the windward slopes. Therefore, the stratiform components of the convective systems are enhanced through gentle orographic lifting by processes similar to those seen over the European Alps when a strong cross-barrier flow of nearly neutral or slightly unstable air rises easily over the mountain barrier and produces heavy orographic rainfall (Houze *et al.*, 2001; Medina and Houze, 2003; Rotunno and Houze, 2007). The formation of convective *systems containing broad stratiform echo* in the eastern Himalayan region is presumably the result of a combination of factors: enhanced moisture due to wind-induced surface heat exchange over the upstream ocean, the enhancement of low-level moisture by diurnal heating of the wetlands, the development of stratiform regions from the aging and merging of repeated convective cells that form over and upstream of the lower windward barrier, and the enhancement of the stratiform region by orographic lifting of the near-moist-adiabatic stratiform clouds.

Acknowledgements

The authors acknowledge Richard Rotunno and two anonymous reviewers for their suggestions. Ulrike Romatschke provided helpful insights and compiled the climatology shown in Figure 3(b). Mark Stoelinga provided assistance in the use and modification of the RIP software package. Stacy Brodzik provided data managing support. Beth Tully edited the manuscript and drafted the figures. The first and

second authors were sponsored by National Science Foundation (NSF) Grants ATM-0505739 and ATM-0820586 and by National Aeronautics and Space Administration (NASA) PMM Award NNX07AD59G. The third and fourth authors received support from NSF-CAREER 0847472 (Liming Zhou and Jay Fein), NASA (NNG05GQ47G Dr. J. Entin; NNG04GL61G Dr. J. Entin and Dr. G. Gutman), and the Purdue University Asian Initiative Program. Computing resources for this study were provided by the National Center for Atmospheric Research, which is sponsored by NSF.

References

Adler RF, Huffman GJ, Bolvin DT, Curtis S, Nelkin EJ. 2000. Tropical rainfall distributions determined using TRMM combined with other satellite and rain gauge information. *J. Appl. Meteorol.* **39**: 2007–2023.

Annamalai H, Slingo JM, Sperber KR, Hodges K. 1999. The mean evolution and variability of the Asian summer monsoon: Comparison of ECMWF and NCEP–NCAR reanalyses. *Mon. Weather Rev.* **127**: 1157–1186.

Betts AK. 1986. A new convective adjustment scheme. Part I: Observational and theoretical basis. *Q. J. R. Meteorol. Soc.* **112**: 677–691.

Betts AK, Miller MJ. 1986. A new convective adjustment scheme. Part II: Single column tests using GATE wave, BOMEX, ATEX and arctic air-mass data sets. *Q. J. R. Meteorol. Soc.* **112**: 693–709.

Bhowmik SKR, Roy SS, Kundu PK. 2008. Analysis of large-scale conditions associated with convection over the Indian monsoon region. *Int. J. Climatol.* **28**: 797–821.

Bougeault P, Binder P, Buzzi A, Dirks R, Houze RA Jr, Kuettner J, Smith RB, Steinacker R, Volkert H. 2001. The MAP Special Observing Period. *Bull. Am. Meteorol. Soc.* **82**: 433–462.

Carlson TN, Benjamin SG, Forbes GS, Li Y-F. 1983. Elevated mixed layers in the regional severe storm environment: Conceptual model and case studies. *Mon. Weather Rev.* **111**: 1453–1474.

Chang H-I, Kumar A, Niyogi D, Mohanty UC, Chen F, Dudhia J. 2009. The role of land surface processes on the mesoscale simulation of the July 26, 2005 heavy rain event over Mumbai, India. *Global and Planetary Change* **67**: 87–103.

Chiao S, Barros AP. 2007. A numerical study of the hydrometeorological dryline in northwest India during the monsoon. *J. Meteorol. Soc. Jpn* **85A**: 337–361.

Douglas EM, Niyogi D, Frolking S, Yeluripati JB, Pielke RA Sr, Niyogi N, Vörösmarty CJ, Mohanty UC. 2006. Changes in moisture and energy fluxes due to agricultural land use and irrigation in the Indian monsoon belt. *Geophys. Res. Lett.* **33**: L14403, DOI:10.1029/2006GL026550.

Ducrocq V, Nuissier O, Ricard D, Lebeaupin C, Thouvenin T. 2008. A numerical study of three catastrophic precipitating events over southern France. II: Mesoscale triggering and stationarity factors. *Q. J. R. Meteorol. Soc.* **134**: 131–145.

Dudhia J. 1989. Numerical study of convection observed during the Winter Monsoon Experiment using a mesoscale two-dimensional model. *J. Atmos. Sci.* **46**: 3077–3107.

Dudhia J. 1996. 'A multi-layer soil temperature model for MM5.' *Preprints, Sixth PSU/NCAR Mesoscale Model Users' Workshop*.

Emanuel KA. 1986. An air–sea interaction theory for tropical cyclones. Part I: Steady-state maintenance. *J. Atmos. Sci.* **43**: 585–605.

Emanuel KA. 1987. An air–sea interaction model of intraseasonal oscillations in the Tropics. *J. Atmos. Sci.* **44**: 2324–2340.

Emanuel KA, Neelin JD, Bretherton CS. 1994. On large-scale circulations in convecting atmospheres. *Q. J. R. Meteorol. Soc.* **120**: 1111–1143.

Godbole RV. 1977. The composite structure of the monsoon depression. *Tellus* **29**: 25–40.

Goswami BN. 1987. A mechanism for the west-north-west movement of monsoon depressions. *Nature* **326**: 376–378.

Goswami BN, Rajagopal EN. 2003. Indian Ocean surface winds from NCMRWF analysis as compared to QuickSCAT and moored buoy winds. *J. Earth Syst. Sci.* **112**: 61–77.

Goswami BN, Sengupta D. 2003. A note on the deficiency of NCEP/NCAR reanalysis surface winds over the equatorial Indian Ocean. *J. Geophys. Res.* **108**(C4): 3124, DOI:10.1029/2002JC001497.

Grossman RL, Durran DR. 1984. Interaction of low-level flow with the Western Ghat mountains and offshore convection in the summer monsoon. *Mon. Weather Rev.* **112**: 652–672.

Hirose M, Nakamura K. 2002. Spatial and seasonal variation of rain profiles over Asia observed by spaceborne precipitation radar. *J. Climate* **15**: 3443–3458.

Hong S-Y, Lim J-OJ. 2006. The WRF single-moment 6-class microphysics scheme (WSM6). *J. Korean Meteorol. Soc.* **42**: 129–151.

Hong S-Y, Pan H-L. 1996. Nonlocal boundary layer vertical diffusion in a medium-range forecast model. *Mon. Weather Rev.* **124**: 2322–2339.

Hong S-Y, Dudhia J, Chen S-H. 2004. A revised approach to microphysical processes for the bulk parameterization of clouds and precipitation. *Mon. Weather Rev.* **132**: 103–120.

Houze RA Jr. 1997. Stratiform precipitation in regions of convection: A meteorological paradox? *Bull. Am. Meteorol. Soc.* **78**: 2179–2196.

Houze RA Jr, Churchill DD. 1987. Mesoscale organization and cloud microphysics in a Bay of Bengal depression. *J. Atmos. Sci.* **44**: 1845–1868.

Houze RA Jr, James CN, Medina S. 2001. Radar observations of precipitation and airflow on the Mediterranean side of the Alps: Autumn 1998 and 1999. *Q. J. R. Meteorol. Soc.* **127**: 2537–2558.

Houze RA Jr, Wilton DC, Smull BF. 2007. Monsoon convection in the Himalayan region as seen by the TRMM precipitation radar. *Q. J. R. Meteorol. Soc.* **133**: 1389–1411.

Huffman GJ, Adler RF, Bolvin DT, Gu G, Nelkin EJ, Bowman KP, Hong Y, Stocker EF, Wolff DB. 2007. The TRMM Multisatellite Precipitation Analysis (TMPA): Quasi-global, multiyear, combined-sensor precipitation estimates at fine scales. *J. Hydrometeorol.* **8**: 38–55.

Iguchi T, Kozu T, Meneghini R, Awaka J, Okamoto K. 2000a. Rain-profiling algorithm for the TRMM precipitation radar. *J. Appl. Meteorol.* **39**: 2038–2052.

Iguchi T, Meneghini R, Awaka J, Kozu T, Okamoto K. 2000b. Rain profiling algorithm for TRMM precipitation radar data. *Adv. Space Res.* **25**: 973–976.

Kalnay E, Kanamitsu M, Kistler R, Collins W, Deaven D, Gandin L, Iredell M, Saha S, White G, Woollen J, Zhu Y, Leetmaa A, Reynolds R, Chelliah M, Ebisuzaki W, Higgins W, Janowiak J, Mo KC, Ropelewski C, Wang J, Jenne R, Joseph D. 1996. The NCEP/NCAR 40-year reanalysis project. *Bull. Am. Meteorol. Soc.* **77**: 437–471.

Kumar A, Dudhia J, Rotunno R, Niyogi D, Mohanty UC. 2008. Analysis of the 26 July 2005 heavy rain event over Mumbai, India using the Weather Research and Forecasting (WRF) model. *Q. J. R. Meteorol. Soc.* **134**: 1897–1910.

McPhaden MJ, Meyers G, Ando K, Masumoto Y, Murty VSN, Ravichandran M, Syamsudin F, Vialard J, Yu L, Yu W. 2009. RAMA: The research moored array of African–Asian–Australian monsoon analysis and prediction. *Bull. Am. Meteorol. Soc.* **90**: 459–480.

Medina S, Houze RA Jr. 2003. Air motions and precipitation growth in Alpine storms. *Q. J. R. Meteorol. Soc.* **129**: 345–371.

Mlawer EJ, Taubman SJ, Brown PD, Iacono MJ, Clough SA. 1997. Radiative transfer for inhomogeneous atmosphere: RRTM, a validated correlated-k model for the longwave. *J. Geophys. Res.* **102**: 16663–16682.

Niyogi DDS, Pielke RA Sr, Alapaty K, Eastman J, Holt T, Mohanty UC, Raman S, Roy TK, Xue YK. 2002. 'Challenges of representing land-surface processes in weather and climate models over Tropics: Examples over the Indian subcontinent.' Pp 132–145 in *Weather and climate modeling*, Singh SV, Basu S, Krishnamurti TN (eds.). New Age International (P) Ltd. Publishers: New Delhi.

Nuissier O, Ducrocq V, Ricard D, Lebeaupin C, Anquetin S. 2008. A numerical study of three catastrophic precipitating events over southern France. I: Numerical framework and synoptic ingredients. *Q. J. R. Meteorol. Soc.* **134**: 111–130.

Rafiuddin M, Uyeda H, Islam MN. 2010. Characteristics of monsoon precipitation systems in and around Bangladesh. *Int. J. Climatol.* DOI: 10.1002/joc.1949, in press.

Rajagopal EN, Harenduprakash L, Mitra AK, George JP. 2001. *'Description of the analysis and forecast data produced by NCMRWF for experimental ocean state forecast.'* Technical note NCMRWF/OSF/1.

Ramage CS. 1971. *Monsoon meteorology*. *International Geophysics Series* 15. Academic Press.

Romatschke U, Medina S, Houze RA Jr. 2010. Regional, seasonal, and diurnal variations of extreme convection in the south Asian region. *J. Climate* **23**: 419–439.

Rotunno R, Houze RA Jr. 2007. Lessons on orographic precipitation from the Mesoscale Alpine Programme. *Q. J. R. Meteorol. Soc.* **133**: 811–830.

Sawyer JS. 1947. The structure of the intertropical front over N. W. India during the S. W. monsoon. *Q. J. R. Meteorol. Soc.* **73**: 346–369.

Schumacher C, Houze RA Jr. 2003. Stratiform rain in the Tropics as seen by the TRMM precipitation radar. *J. Climate* **16**: 1739–1756.

Sikka DR. 1977. Some aspects of the life history, structure and movement of monsoon depressions. *Pure Appl. Geophys.* **115**: 1501–1529.

Sivall TR. 1977. Synoptic–climatological study of the Asian summer monsoon in Afghanistan. *Geografiska Annaler, Series A, Physical Geography* **59**: 67–87.

Skamarock WC, Klemp JB, Dudhia J, Gill DO, Barker DM, Wang W, Powers JG. 2005. '*A description of the Advanced Research WRF Version 2*.' NCAR Tech. Note., NCAR/TN-468+STR, 88 pp. Available from UCAR Communications, PO Box 3000, Boulder, CO 80307, USA.

Swain D, Rahman SH, Ravichandran M. 2009. Comparison of NCEP turbulent heat fluxes with *in situ* observations over the south-eastern Arabian Sea. *Meteorol. Atmos. Phys.* **104**: 163–175.

Webster PJ. 2006. The coupled monsoon system. Pp 3–66 in *The Asian monsoon*, Wang B (ed). Springer Praxis: Chichester, UK.

Xie S-P, Xu H, Saji NH, Wang Y, Liu WT. 2006. Role of narrow mountains in large-scale organization of Asian monsoon convection. *J. Climate* **19**: 3420–3429.

Xu K-M, Emanuel KA. 1989. Is the tropical atmosphere conditionally unstable? *Mon. Weather Rev.* **117**: 1471–1479.

Yano J-I, Emanuel KA. 1991. An improved model of the equatorial troposphere and its coupling with the stratosphere. *J. Atmos. Sci.* **48**: 377–389.

Zipser EJ, Cecil DJ, Liu C, Nesbitt SW, Yorty DP. 2006. Where are the most intense thunderstorms on Earth? *Bull. Am. Meteorol. Soc.* **87**: 1057–1071.

